Prediction of Tunnel Squeezing in Soft Sedimentary Rocks by Geoelectrical Data

Mohammadreza Akbariforouz[1,2*], Qi Zhao[2,], Reza Taherdangkoo[3], Alireza Baghbanan[4], Christoph Butscher[3], Chunmiao Zheng[1,5]**

[1]EIT Institute for Advanced Study, Ningbo, China;

[2]Department of Civil and Environmental Engineering, The Hong Kong Polytechnic University, Hung Hom, Kowloon, Hong Kong, China;

[3]TU Bergakademie Freiberg, Institute of Geotechnics, Gustav-Zeuner-Str. 1, 09599, Freiberg, Germany;

[4]Department of Mining Engineering, Isfahan University of Technology (IUT), Isfahan, Iran

[5]Environmental Protection Key Laboratory of Integrated Surface Water-Groundwater Pollution Control, School of Environmental Science and Engineering, Southern University of Science and Technology, Shenzhen, China;

*Corresponding author: mo2022.akbariforouz@connect.polyu.hk

** qi.qz.zhao@polyu.edu.hk

Abstract: Squeezing is time-dependent deformation that can cause technical difficulties and financial consequences in underground structures. This study employs electrical resistivity data to predict squeezing intensity along the Beheshtabad tunnel in the Sanandaj-Sirjan zone in Iran. For comparison analysis, a semi-empirical approach was correlated with numerical modeling to predict tunnel squeezing at the design stage. The squeezing intensity obtained for the Beheshtabad tunnel was then compared with the instability observations along the Golab tunnel excavated in sedimentary rocks of the same zone. We developed a relationship between

electrical resistivity and strains and provided a new strain-based squeezing classification system. The calibrated electrical data produced more accurate results for predicting tunnel squeezing than the conventional methods. The results show that rock type, joint properties, and water saturation impact squeezing.

Keywords: Squeezing; Electrical resistivity; Semi-empirical approach; Strain-based classification system

List of symbols

ER	Calibrated electrical resistivity	Ohm.m
*ER**	Electrical resistivity	
CRP	Continuous resistivity profiling	-
σ_{cm}	Uniaxial compressive strength of rock mass	MPa
σ_v	Vertical in-situ stress	MPa
ε	Normalized strain	%
ε_{cr}	Critical strain	%
RMi	Rock Mass index	-
σ_Θ	Tangential stress	MPa
BH	Borehole	-
CRP	Continuous resistivity profiling	-
AB	The maximum flow line	-
RMSQ	Root squared error	%
PPM	Proton Procession Magnetometer	-
Q	Quality Index	-
GSI	Geological strength index	-
E_{rm}	Rock mass deformation modulus	GPa
σ_{ci}	Uniaxial compressive strength of intact rock	MPa
E_i	Elastic modulus of intact rock	GPa
v	Poison ratio of intact rock	-
C_{rm}	The cohesion of rock mass	MPa
ϕ_{rm}	Friction angle of rock mass	°
v_{rm}	Poison ratio of rock mass	-
SI	Squeezing index	-
γ	Unit weight	kN/m^3
u_a	Radial closure	m
a	The opening radius of tunnels	m
E^c	Conglomerate	
$\boldsymbol{K_4^{s,sh}}$	Siltstone & shale	

K_4^{sh}	Shale	
K_4^{lsh}	Limy shale	
PL-Q_b^m	Mudstone	
PL-Q_b^c	Bakhtiary conglomerate	
OM_a^l	Assemary limestone	
M_r^m	Razak marlstone	
K	Stress ratio (s)	-
K_h	Minimum stress ratio	
K_H	Maximum stress ratio	
K_{hH}	Equivalent stress ratio ($K_H \times K_h$)	
z	Tunnel depth	m
D	Disturbance factor	-
σ_H & σ_h	Horizontal stress components	MPa
ρ	Density	kg/m^3
FDM	Finite difference method	-
N	No squeezing state	-
L	Light squeezing state	-
M	Moderate squeezing state	-
S	Severe squeezing state	-
VS	Very severe squeezing state	-

1. Introduction

Time-dependent rock deformations due to disturbance of the primary stress field can impose high pressure on support installations, especially in deep tunnels excavated in soft rocks (Swannell et al., 2016). This type of deformation, called squeezing, can continue during the construction phase or even over a long period. This phenomenon is crucial for mechanized tunneling (Barla & Barla, 2008).

Squeezing is more common in relatively deep underground structures excavated in soft rocks. However, this phenomenon can occur (due to topographic or tectonic conditions) for weak rocks at shallow depths (Shrestha & Broch, 2008) and in deep tunnels excavated in hard rocks (Malan, 1999). Predicting squeezing

potential around underground structures is a challenging task, especially in the design phase, and requires a deep understanding of rock mass behavior.

Squeezing problems have been recorded in many tunnels, e.g., the San Bernardino and Gotthard road tunnels in Switzerland (Thut et al., 2000) and the second part of the water-supply Karaj tunnel in Iran (Khanlari et al., 2012). Some previous studies also included comprehensive databases for various squeezing cases (Feng and Jimenez, 2015; Sun et al., 2018; Chen et al., 2020).

Geotechnical equations and exploration approaches can provide a comprehensive perception of rock mass conditions and evaluate deformations of excavated tunnels. Geotechnical (conventional) methods are classified as empirical and semi-empirical equations (e.g., Hoek & Marinos, 2000; Palmström, 2001) and physics-based numerical modeling (Hasanpour et al., 2014). These equations are usually obtained based on a few geotechnical parameters that can affect squeezing. For example, the Aydan approach was derived from some tunnels excavated in Japan (Aydan et al., 1996). Applying geotechnical equations can provide erroneous results when geotechnical parameters are uncertain (i.e., in the design phase).

Empirical equations are developed based on rock mass classification indices (Singh et al., 1992; Goel et al., 1995), while semi-empirical equations are provided based on deformations. Empirical equations determine squeezing occurrence based on rock mass indices, e.g., using the Norwegian rock mass classification index (Singh et al., 1992). Thus, their results cannot be compared to semi-empirical approaches, which predict the squeezing intensity. Semi-empirical equations employ different ratios: e.g., the uniaxial compressive strength of rock mass to vertical in-situ stress (Jethwa et al. 1984), the calculated strain to critical strain (Aydan et al., 1996), the rock mass index (*RMi*) to induced tangential stress (Palmstrom, 2001) and the uniaxial compressive strength of rock mass to strains (Hoek & Marinos, 2000).

Physics-based numerical modeling can cover a large-scale medium. However, a proper numerical approach is required that can simulate coupled processes to predict squeezing potential. Numerical modeling was previously used to evaluate deformations and squeezing, e.g., by incorporating elasto-viscoplastic models into numerical tools to simulate time-dependent deformations (Barla et al., 2012; Hasanpour et al., 2014).

The accuracy of numerical models can be affected by uncertain geotechnical data and modeling simplifications, particularly at the design stage.

The exploration approaches (including laboratory experiments, in-situ tests, and geophysical prospecting) can also be used to evaluate squeezing. In-situ tests can cover larger areas comparing laboratory experiments, i.e., the tested area is excavated galleries instead of drilled boreholes. However, laboratory experiments and in-situ tests can cover the study site partially.

Geophysical data can be a practical approach to determining the rock mass condition at a large scale. This approach has been employed to assess site characteristics of roads, dams, offshore installations, slopes, and ancient sites (e.g., Akinrinmade et al., 2013; Whiteley, 2006). Geoelectrical data have not been considered as an index to detect underground deformations. Geoelectrical prospecting (i.e., relying on electrical resistivity contrasts of different geomaterials) was frequently used (Ammar & Kamal, 2018).

The geotechnical and geophysical parameters (especially *ER*) are usually momentary and time-independent. However, the main difference between the *ER* and geotechnical data is the coverage area; i.e., geotechnical properties are based on drilled boreholes and can be uncertain at the design stage. Complementary geotechnical data at the production phase usually alter the initial geotechnical data.

One challenging task in predicting squeezing was the time-dependent behavior of rock mass. All previous studies used indices such as rock mass classification systems (Jimenez & Recio, 2011; Dwivedi et al., 2013) or geotechnical parameters (Aydan et al., 1996; Hoek & Marinos, 2000) as an indirect scale of the time-dependent behavior. The driving force behind this indirect application was the possibility to define time-dependent deformation using fractures properties (e.g., weathering, orientation, spacing, filling materials, roughness, and water inflow) and geotechnical characteristics (including rock mass uniaxial compressive strength and overburden). Using joint properties and geotechnical conditions to predict squeezing at the design stage was limited to numerical modeling, e.g., correlating a simple numerical model and a semi-empirical equation to predict the squeezing (Khanlari et al., 2012).

The squeezing intensity is substantially related to rock composition and structure, and rocks with significant clay minerals (e.g., claystone, shale, siltstone, mudstone, marlstone) and a water-bearing porous medium are susceptible to tunnel squeezing (Kovari & Staus, 1996; Aceh, 2019; Arora et al., 2020).

The relationships between rock strength parameters and squeezing were studied (Aydan et al., 1996; Vrakas, 2017; Wood, 1972). Under high overburden pressure, the ratio of rock strength to in-situ stress decreased, and the squeezing potential increased (Gutierrez & Xia, 2008; Jethwa et al., 1984; Hoek & Marinos, 2000). Field observations revealed the direct effect of groundwater conditions and stress on squeezing (Arora et al., 2020; Sun et al., 2018).

In the case of fracture effects, a few squeezing approaches were developed based on the frequency and properties of discontinuities (Singh et al., 1992; Goel et al., 1995; Jimenez & Recio, 2011; Dwivedi et al., 2013). Saturated weak rocks can deteriorate over time. This weakening process can also be related to weathering. Similar to weathering, the initiation and development of cracks can increase the squeezing intensity (Agan, 2015).

Other factors that can affect squeezing, albeit to a lesser extent (Sun et al., 2018), are the installed support system as well as methods and rates of excavation, mainly related to decisions at the production phase (Sun et al., 2018), and are out of the scope of this research.

The prementioned factors can alter *ER*. The *ER* value of rocks with high clay compositions or porous rocks (with high water content) is low (Kovari & Staus, 1996). Laboratory experiments, field data, and numerical modeling confirmed the relationship between parameters affecting *ER* and squeezing (Ammar & Kamal, 2018) (**Figure 1**). For example, the fluid-bearing capacity (Bhatt & Jain, 2014), fluid pressure, weathering, fracture characteristics, faults activations (Backstrom, 2004; Laszlo, 2011), porosity, and lithology of rock matrix (Aceh, 2019) can influence *ER*, similar to tunnel squeezing. For saturated rock specimens, alterations of *ER* are related to high vertical stress during experimental studies in plastic deformation zone (Brace & Orange, 1968; Dayuan et al., 1988). However, lower *ER* values show a higher squeezing intensity.

Water exploitation by geoelectrical prospecting is a frequently-used method (Ammar & Kamal, 2018; Rolia & Sutjiningsih, 2018). At the deformation zone, *ER* changes are due to the volume increase under

shear deformations and micro-crack development (Chen & Lin, 2004). The decreasing trend of *ER* due to fracture propagation, including the effects of crack frequency, was also detected (Li et al., 2015; Sandler et al., 2009).

The higher the overburden, rock strength, and fracture density are, the lower the *ER* is. Therefore, the relationship between these parameters and squeezing intensity is direct. Water saturation can also decrease *ER*. A combination of porosity, water-bearing capacity, structure, and mineralogy affect *ER* (and rock squeezing).

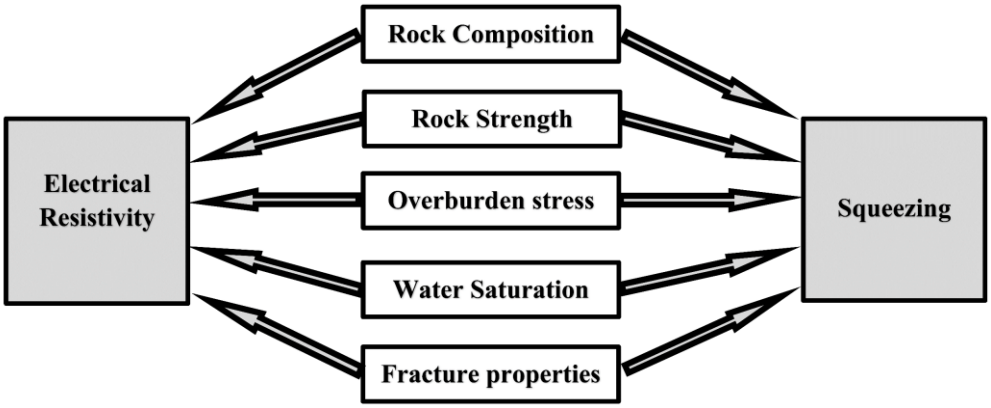

Figure 1: The factors controlling (before excavation) *ER* and squeezing are presented. The factors decrease *ER* while increasing the squeezing intensity.

This study aims to predict the time-dependent behavior of rock mass based on *ER*, which may provide remarkable insight into the general situation of joints and rock mass. The in-common factors affecting squeezing and *ER* confirmed the correlation between rock squeezing and *ER*.

The chainage of 7.6-16 km of the Beheshtabad tunnel in the Sanandaj-Sirjan zone is prone to the squeezing phenomenon. We compared the predicted squeezing with observational data (obtained from chainage of 0-8.8 km of the Golab tunnel excavated in the sedimentary rocks of the same geological zone). Then we developed a relationship between *ER* and squeezing based on in-situ strain measurements of strain during the excavation of the Golab tunnel. This research also compared the prediction accuracy of the combined semi-empirical and numerical modeling to the *ER*-based approach.

2. Methodology

Two approaches were chosen to predict the squeezing potential along sedimentary rocks of the Behesht-abad and Golab tunnels: (1) a combination of numerical modeling and a semi-empirical approach and (2) geoelectrical prospecting. The observational data obtained during the excavation of the Golab tunnel were also employed for the comparison analysis. A relationship was defined between calibrated electrical data and in-the-field measured strains recorded in excavating the Golab tunnel, and the squeezing intensity along the Behehstabad study site was predicted by the developed approach.

2.1. Description of the study sites

The Beheshtabad tunnel is located in the Chaharmahal-Bakhtiari province in Iran, planned to convey water from the Beheshtabad dam to the Central Plateau of Iran. The tunnel has a northeast trend and ends in the Zayanderoud River upstream of Cham Aseman dam. The length (total) and diameter of the Behehstabad tunnel are 64.97 km and 6.8 m, respectively.

The Beheshtabad study site, chainage 7.6-16 km, is located in the Sanandaj-Sirjan zone, in the Zagros and Naien-Baft Orogen of Gondwanan provenance (Fergusson et al., 2016; Ghasemi & Talbot, 2006). This zone (as a metamorphic belt) is affected by several geological and tectonic events: continental collision (late Eocene-early Miocene), Pan-African orogenesis, Late Palaeozoic rifting forming Neo-Tethys, Mesozoic convergence, and ophiolite obduction (Fergusson et al., 2016; Ghasemi & Talbot, 2006). **Figure 2a** shows the location of the Beheshtabad tunnel as the dashed blue line and the study site as the red rectangle. The topographic and geophysical profiles of the study site are shown in **Figure 2b**.

The Sanandaj-Sirjan zone (with a width of 150-200 km) extends 1500 km from Sanandaj (in the north) to Sirjan city in the south. Paleozoic volcanic rocks, including Silurian, Devonian, and Permian rocks with intrusions of Mesozoic rocks and the metamorphism due to Cimmerian movements, are the main features of this zone. The zone is evolved dynamically by the Neotethys Ocean movements at the northeastern margin of Gondwana (Ghazi & Moazzen, 2015). It is mainly composed of sedimentary rocks, including limestone, marlstone, siltstone, mudstone, shale, and conglomerate (Zayandab, 2006 & 2010).

To estimate the behavior of the Beheshtabad study site during excavation, a chainage of the Golab tunnel (0-8.8 km), excavated in sedimentary rocks of the Sanandaj-Sirjan zone, was evaluated. Several instability failures, tunnel collapses, and squeezing damages were recorded in this tunnel; these observations were employed to predict the squeezing along the study site of the Beheshtabad tunnel (planned to be excavated).

The total length and diameter of the Golab tunnel are 17.02 km and 4.6 m, respectively. The support system was installed 1 m away from the face. The temporary and permanent support systems of the Golab tunnel were a 5 cm shotcrete layer reinforced with wire mesh and a 25 cm lining, respectively. In sections with severe squeezing problems, steel sets were also added to the temporary support system (Zayandab, 2006). The mechanized tunneling using an open-shield TBM was planned for the Beheshtabad tunnel. The suggested support system was a 10 cm shotcrete layer reinforced with wire mesh as the temporary and a 25 cm lining as the permanent support system (Zayandab, 2010). Therefore, the support systems of both study sites were designed almost similarly.

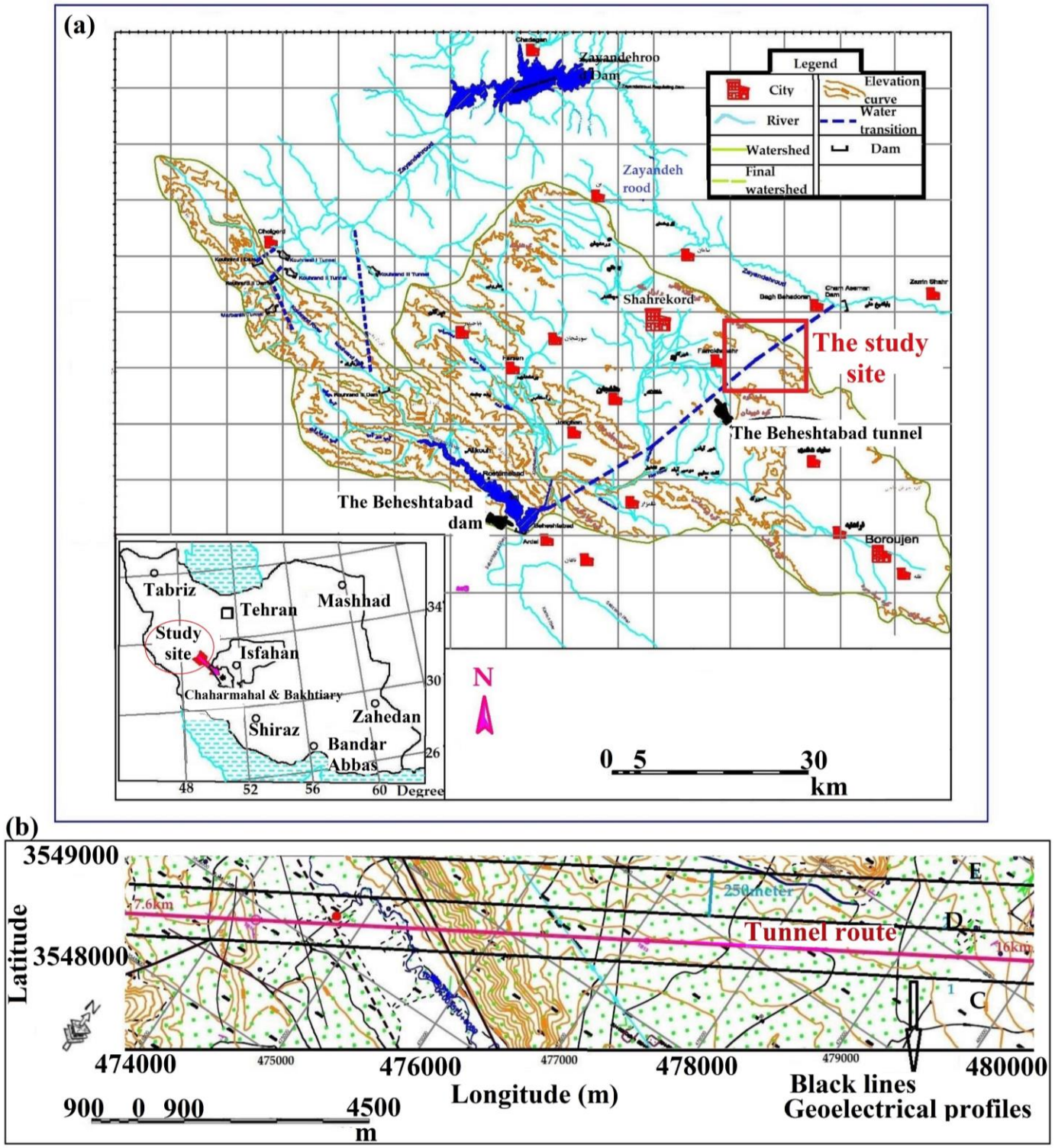

Figure 2: (a) The location of the Beheshtabad tunnel in the central plateau of Iran. The red rectangle depicts the study site, i.e., 7.6-16 km. (b) The tunnel route (pink line) and geoelectrical profiles (black lines: C, D, and E) are shown by the black arrow (Zayandab, 2010).

Figure 3 illustrates geological profiles and drilled boreholes along the Golab and Beheshtabad tunnels. The axis of both tunnels is located below the water table. Eight boreholes were drilled along the Golab tunnel (**Figure 3a**) and four boreholes along the Beheshtabad tunnel (**Figure 3b**).

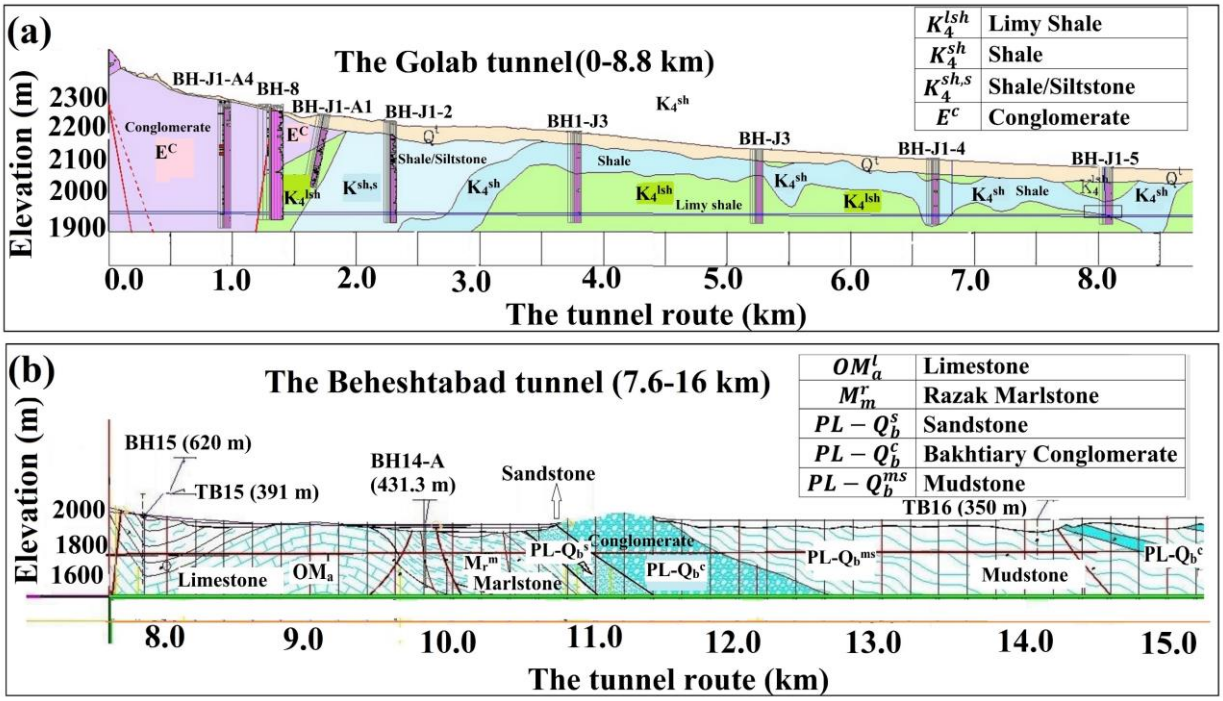

Figure 3: The geological profiles of the study sites: (a) the Golab tunnel (0 to 8.8 km). (b) the Beheshtabad tunnel (7.6-16 km). The blue and brown lines are symbols of the tunnel axis (Zayandab, 2006 and 2010). BH-J is representative of the boreholes excavated along the Golab tunnel, while BH and TB depict the boreholes for the Beheshtabad tunnel. The symbols of the geological units (e.g., E^c) are defined in **Table 1**. The profiles along the boreholes (**Figure 3a**) present the *RQD* values along their lengths.

For chainage 0-8.8 km of the Golab tunnel, various squeezing problems were mainly recorded for formations with a high amount of clay, including siltstone and shale. A comprehensive set of data was recorded during the excavation of this tunnel along 2 m sections, including the joint properties, fault activations, groundwater condition, weathering, electrical resistivity, and squeezing intensity. The water table is about 150 m above the tunnel axis.

At the chainage of 0-1120 m, a conglomerate formation (E^c) (good rock based on *RMR* index) and hydraulic flux of 1.5×10^{-7} to 1×10^{-6} m/s was detected. The squeezing was limited to light cases (from the

tunnel inlet to about 500 m). This squeezing was mainly tectonic-based, related to the branches of Fault Abrizan-Kamason. Water penetration (due to relatively high hydraulic conductivity) was also recorded (Zayandab, 2006).

Light squeezing phenomena occurred in chainage 1210-1550 m, mainly related to fracture zones at limy shale. The squeezing in K_4^{lsh} (in sections 3050-6570 m, 6800-8100 m, and 8570-8800 m) was also recorded, especially at 6312-6570 and 7560-8100 m moderate squeezing cases were mainly related to fault activations (Zayandab, 2006).

The most challenging squeezing problems occurred in 1550-2730 m in a rock mass with high clay content (i.e., $K_4^{sh,s}$); numerous cases of M (moderate) to VS (very severe squeezing) were observed. The hydraulic flux was measured from 1×10^{-9} to 2×10^{-8} m/s (Zayandab, 2006).

Shale rock mass (K_4^{sh}) was detected in sections 2730-3050 (light squeezing), 6570-6800 (moderate squeezing), and 8100-8570 m (severe squeezing problems due to the activation of faults). The hydraulic flux of K_4^{sh} and K_4^{lsh} was measured between 3×10^{-9} to 2×10^{-7} m/s (Zayandab, 2006).

Along the Beheshtabad tunnel, chainages 7600-8120 m and 9630-10790 are Razak marlstones (M_r^m) with relatively low flux (1×10^{-8} to 1×10^{-10} m/s). The *RMR* class is fair to good. Possible risks of squeezing can be related to weathering of marlstones and the fault activations. At 7700 m, a fault was detected. Fault K2 can impact its surrounding marly rock mass at 9600-10000 m (Zayandab, 2010).

From 8120 to 9630 m, Asmary limestone (OM_a^L) (fair to good rock mass) is affected by a branch fault at 8400 m and Fault K2 at 9200-9600 m. Other parts of the rock mass do not show symptoms of weathering based on boreholes, and the flux of rock mass ranges between 1×10^{-9} to 1.7×10^{-7} m/s (Zayandab, 2010).

10790-12110 m chainage mainly consists of Bakhtiary conglomerate (PL-Q_b^c), including sandstone (Q_b^s) at 10790-11100 m. The rock mass condition is fair to good, with no sign of weathering. The hydraulic flux of rock mass is relatively higher, 6×10^{-8} to 1×10^{-6} m/s, and water penetration can be possible. The most squeezing-prone part of this section is around 12100 m, where a branch fault was detected (Zayandab, 2010).

The remaining chainage (12110-16000 m) of the Beheshtabad study site is mainly composed of mudstone (PL-Q_b^{ms}) with a flux of 1.5×10^{-7}-2.7×10^{-7} m/s. At 15600-16000 m, conglomerate rock mass can increase the permeability. Fault Zagros impacts the chainage of 15500 to 16000 m (Zayandab, 2010).

The existence of faults and rock masses with a high amount of clay shows that squeezing problems can be significant along the Beheshtabad tunnel. The groundwater level ranges between 40 and 60 m below the land surface (about 200 m above the tunnel axis).

2.2. Geophysical studies

Geophysical evaluations are essential for geoengineering projects, especially for deep tunnels. The geoelectrical surveys provide several advantages: (1) Detecting geological, hydrogeologic, and geotechnical obscures. (2) Preparing electric resistivity maps. (3) Exploring tectonic factors and recognizing relations between physical and geological conditions. (4) Detecting faults/fractured zones.

In-common effective parameters decrease *ER* while increasing the squeezing intensity, considering the literature review. Before defining a relationship between these two parameters, we should respond to two main challenges: (1) Can we trust the accuracy of *ER*? (2) How a quantitative relationship can be defined between *ER* and squeezing?

We considered a novel idea: predicting tunnel squeezing based on *ER* variations. Nevertheless, the accuracy of this approach can be affected because the structure depth (especially for deep tunnels) can affect the resolution of electrical prospecting (Bernabini et al., 1988). A long electrode distance can also undermine the efficiency of geoelectrical data for deep structures. Meanwhile, subsurface electromagnetic interferences (including conductive mineral masses, underground caves, and water-bearing layers) can influence the data quality due to being detected as sharp resistivity anomalies (Militzer et al., 1979; Rolia & Sutjiningsih, 2018). A single geophysical method can recognize all these anomalies as potential squeezing areas. Therefore, some actions were required to evaluate the data accuracy and to cover the disadvantages of electrical prospecting before predicting squeezing.

Geoelectrical mapping of the Golab site includes a Schlumberger array (**Figure 4a**) along three main profiles and continuous resistivity profiling (CRP) along seven directions. For the main profiles, the maximum flow line was 1000 m, the number of electrodes on each profile was 173, and the electrode distance was 50 m. The multi-electrode method with three electrodes was used for CRP at a 50 m distance (Zayandab, 2006).

At the Beheshtabad study site, the Schlumberger array was performed along three main profiles (C, D, and E) in **Figure 2b**; the CRP profiles, along eight directions. The distance of the main profiles was 250 m, the maximum flow line was 1000 m, and the electrode distance ranged from 50 to 100 m. The three-electrode array was considered for 75 locations for each CRP (Zayandab, 2010).

The inversion method was used to obtain geoelectrical mappings. Res2DInv (a finite element software) inversed the data (Geotomosoft, 2014) based on the Gauss-Newton approach (Sasaki, 1992), and the apparent resistivity data built a two-dimensional model of the study sites. The ground layers were divided into rectangular blocks with constant resistivity values. Block thickness was smaller near the ground surface as the influence of the block thickness on results was lower in terms of the root mean squared error (RMSE) (Loke, 2002).

In the Schlumberger array, the thickness of the first layer of the model is equal to half of the electrode space, i.e., 25 m and 50 m for the Golab and Beheshtabad tunnels, respectively. The thickness of each layer increased by 10 % compared to its top layer (**Figure 4c**). RMSE values for all profiles were almost constant and lower than 7 % after eight iterations (**Figure 4b**). **Figure 5** illustrates the geoelectrical mappings of the study sites.

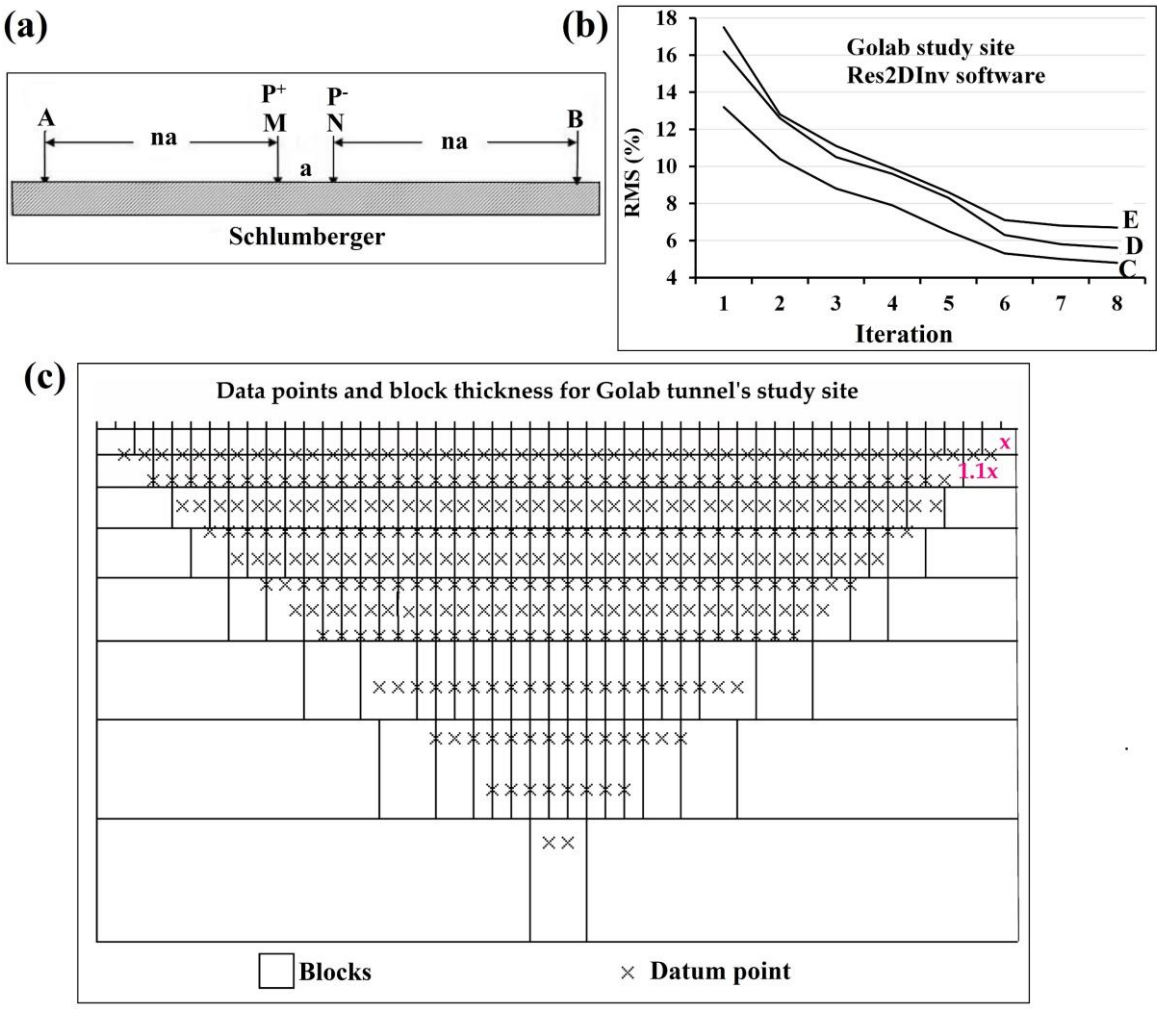

Figure 4: The geoelectrical model of the Golab study site: (a) Schlumberger electrode array where *a* and *na* depict the electrode distance and maximum flow line, respectively, (b) RMSE [%] for the main profiles, and (c) Block discretization scheme used in Res2DInv software. The thickness of each layer increased by 10 % (1.1x) compared to its top layer (x).

In section 7.6-16 km of the Beheshtabad tunnel (from the south in 7.6 km toward the north in 16 km), Asmari limestone (brownish color) was detected in about 400 m, overlaid by Razak marlstone with low resistivity values (the green areas in **Figure** 5a). The resistant zone (the brownish color in chainage 10 to 12 km) is sandstone and Bakhtiary conglomerate, up to deeper than 400 m. A fault in the interface of Razak marlstone and the conglomerate was visible (12 km). Toward the north, the Bakhtiary conglomerate is covered by low-resistant formations of marly-limestone and mudstone between 11500 to 15500 m. *ER* varies

due to fault activations and material contacts toward the outlet. The geoelectrical data were also compared with geological observations on the surface and geotechnical data of the boreholes (Zayandab, 2010).

For the Golab tunnel, in high elevations of the first kilometer of the tunnel route (from the east towards west), *ER* was lower than the value of conglomerate near the tunnel elevation, which was due to the activation of Fault Abrizan-Kamason and the presence of marly layers. The resistivity of siltstone and shale was low (shown by the blue color), and the resistivity of shale was typically lower than limy shale. In Chainage 7.5-8.5 km, *ER* decreased due to fault activations (Zayandab, 2006).

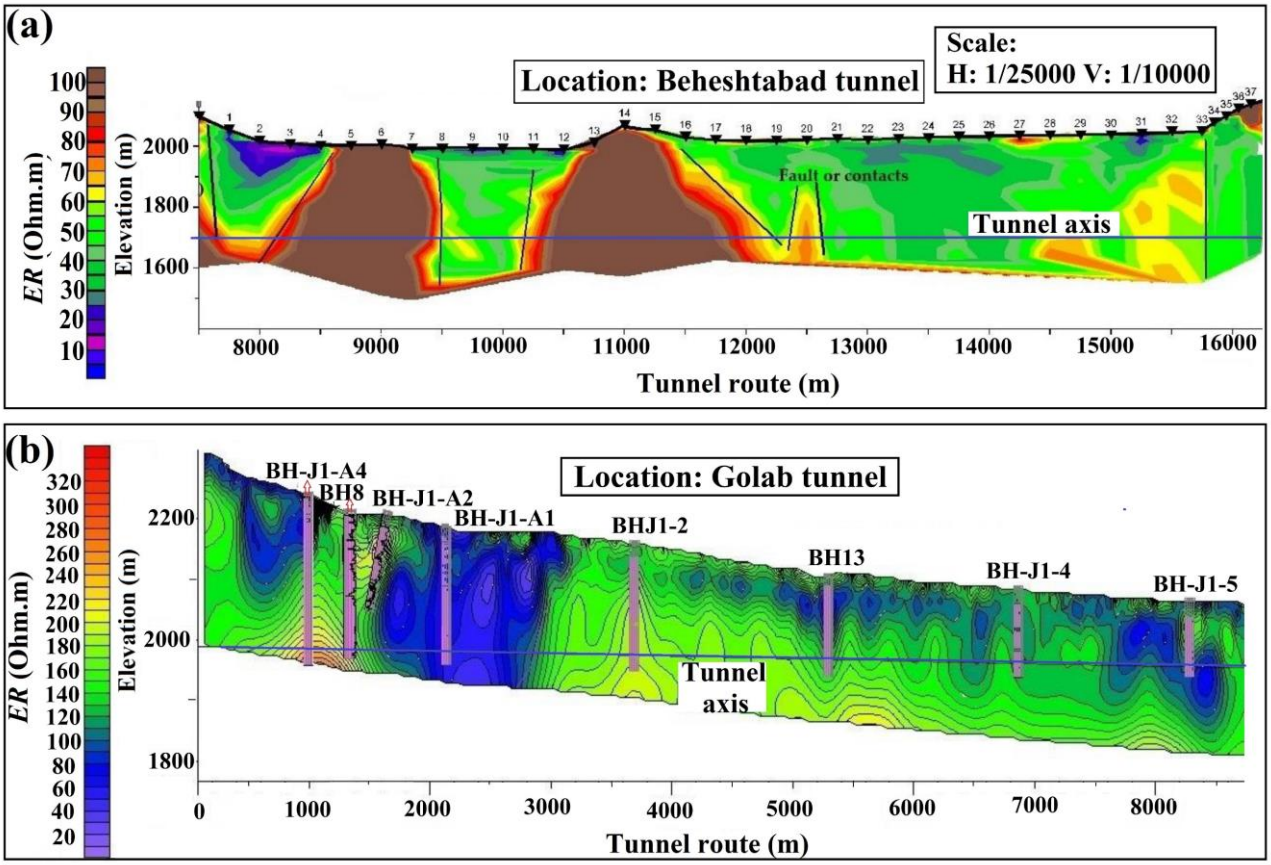

Figure 5: The geoelectrical profiles: (a) the Beheshtabad tunnel, 7.6-16 km (Zayandab, 2010), and (b) the Golab tunnel (0 to 8.8 km) (Zayandab, 2006). For (b), BHi and BH-Ji depict the boreholes.

Before utilizing geoelectrical mappings for predicting squeezing, the efficiency and accuracy of electrical data were evaluated. Influences of the electrode distance on geoelectrical outputs were measured by a sensitivity analysis. The effects of depth on the accuracy of electrical prospecting were also calculated. The multiple geophysical approaches were considered to cover the inability of the geoelectrical method to detect

unrelated anomalies. Gravimetric and magneto-metric methods were performed for Golab and Beheshtabad tunnels to detect misleading anomalies, e.g., conductive minerals, caves, and water-bearing layers (Za-yandab, 2006 and 2010).

The sensitivity analysis was performed based on data collected from different maximum flow lines, i.e., 80, 140, 200, 300, 400, 600, and 800 m. We also used data with an electrode distance of 10 m to determine the effects of electrode distance, depth, and saturation on electrical resistivity. The geoelectrical data were recorded for two sections: the 0-24 km of the Golab tunnel and 0-64.9 km of the Behehstabad tunnel (Za-yandab, 2006 & 2010).

The geological units in **Figures 3** and **5** were also detected at other parts of the tunnels (i.e., 8.8-17 km for the Golab tunnel and 0-7.6 km for the Beheshtabad tunnel). The range of *ER* for geological units was evaluated for the whole lengths of both tunnels to compare the electrical data based on water saturation, depth, and fracture properties. Rock mass classification indices, overburden depth, electrical resistivity, weathering, and water saturation conditions were recorded for all sections. An example of such an analysis is shown for a 2 m section (**Figure 6**) ($K_4^{sh,s}$ in 1550-2730 m of the Golab tunnel).

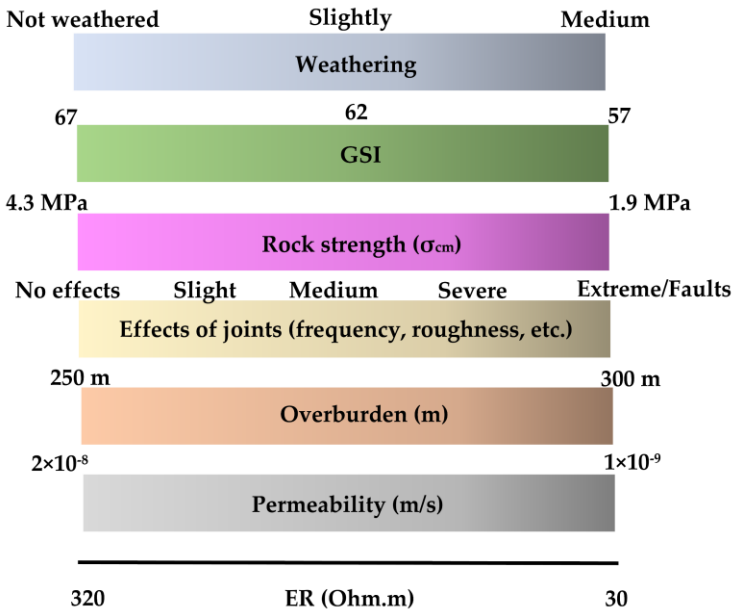

Figure 6: The considered methodology to estimate the accuracy of *ER* values. An example of the results provided by this method is presented. All rock masses were saturated in the studied parts. A lower permeability can also reduce the squeezing potential.

According to **Figure 6**, the factors were sorted from unfavorable to favorable conditions for squeezing potential. The range of ER^* (**Table 1**) was considered for the whole section, and *ER* value was estimated based on each factor. The average value was calculated for 2 m sections with slight weathering (**Figure 6**), e.g., *GSI* = 57 (30 Ohm.m), rock strength of 1.9 MPa (30 Ohm.m), overburden 275 m (145 Ohm.m), permeability 2×10^{-8} m/s (30 Ohm.m), which was impacted by joints (30 Ohm.m), the average value of *ER* was calculated 68 Ohm.m. We compared this estimated value with the *ER* profile for the section and calibrated ER^* values. We prepared similar charts for all 2m sections and geological formations along the tunnels.

This method assumes linear relationships between *ER* and the factors (**Figure 6**). Some of these factors were qualitative parameters. During the design phase, many qualitative scales (such as rock mass classification scales) are usually used based on some assumptions (accepting some errors). We utilized this methodology to control if the *ER* value was reasonable for each section or if it was required to modify *ER**.

The measurements based on a 10 m electrode distance were compared for the chainage 0-3050 m of the Golab tunnel and 8120-15360 m of the Beheshtabad tunnel (Zayandab, 2006 and 2010). These data were also used to calibrate the *ER** of the whole lengths of tunnels. We compared sections with almost similar factors (according to **Figure 6**) at 10 m and 50 m electrode distances and modified *ER** values (in case it was required). For the Beheshtabad tunnel, since the tunnel was not excavated, we used the information on geological units at the surface and borehole data to evaluate each section. The final results of this study were based on the Golab tunnel; therefore, the accuracy of this method was based on the data in the production phase. i.e., we used the calibrated data of the Beheshtabad tunnel for predicting squeezing intensity, not for developing the squeezing predictive criterion.

The average difference between the initial and calibrated (calculated by a 10 m electrode distance and the methodology presented in **Figure 6**) *ER* values was 19.6 % for Beheshtabad and 11.35 % for the Golab tunnel. For example, for shale (K_4^{sh}), the electrical values changed from 30-210 to 20-200 Ohm.m, i.e., an average error of 11 % was detected. The calibrated values were then calculated by averaging electrical values for all geological units along the studied sites, and the initial electrical resistivity values (*ER**) were modified to the calibrated values (*ER*) (Zayandab, 2006 and 2010).

The maximum difference was detected for the Bakhtiary conglomerate in Beheshtabad and the Conglomerate (E^c) in the Golab tunnel. These two units have the maximum overburden, higher than 400 m, which confirmed the effect of depth on the inaccuracy of electrical results. **Table 1** summarizes the geoelectrical data before and after the sensitivity analysis.

Table 1: The initial and calibrated *ER* ranges of Golab (0-17 km) and Beheshtabad (0-16 km) tunnels (Zayandab, 2006 & 2010).

Study site	Geological units	ER^* (Ohm.m)	*ER* (Ohm.m)
Beheshtabad (0-16 km)	Coarse-grained alluvium	320-1000	300-1000
	Medium-grained alluvium	110-310	100-300
	Fine-grained alluvium	50-100	50-100
	Mudstone ($PL\text{-}Q_b^{ms}$)	40-140	20-110
	Bakhtiary conglomerate ($PL\text{-}Q_b^{c}$)	70-340	50-300
	Limestone/sandstone (OM_a^l/Q_b^s)	80-650	50-600
	Razak marlstone (M_r^m)	40-130	20-120
Golab (0-17 km)	Alluvial sediments (medium-grained)	20-350	10-350
	Conglomerate (E^c)	160-650	100-600
	Shale/siltstone ($K_4^{sh,s}$)	30-320	20-300
	Shale (K_4^{sh})	30-210	20-200
	Limy shale (K_4^{lsh})	80-520	80-500

The proton precession magnetometer (Scintrex Co.) with a sensibility of 0.1 nT recorded the magnetometric data (nanoscopic alterations of the magnetic field). The nuclear magnetic resonance of the earth was checked, reaching a 500 m depth. This device was used to locate the possible existence of igneous masses,

faults, conductive minerals, and other anomalies (Howland-rose, 1981). CG-3 automated gravity meter evaluated the gravimetric variations (Scintrex limited, 1995) along three profiles (with a reading resolution of 0.001 mGal) with a 50 m distance to detect sharp density contrasts, e.g., the presence of the water-bearing structures or cavities (Zayandab, 2006 & 2010), up to the depth of 500 m.

The prementioned complementary and calibrating methods increased the accuracy of *ER* data. Then, we used the data to predict squeezing potential at the design stage. Therefore, we answered the second challenging question of our predictive model: *ER* alterations can be considered a relatively accurate scale to predict squeezing after calibration. Hence, the remained challenge was defining a relationship between *ER* and squeezing.

2.3. Geotechnical studies

A series of laboratory experiments were conducted on prepared samples according to the ISRM standards (ISRM, 1977a, 1977b & 1978) to determine geotechnical characteristics of the study sites, including porosity, density, uniaxial and triaxial compression strengths. The properties of rock joints (such as weathering and roughness) were also recorded (Zayandab, 2006 & 2010). The rock mass characteristics and classifications indices-including quality index (*Q*) and geological strength index (*GSI*)-were calculated based on the properties of intact rocks and rock joints. The geological properties of the study sites are shown in **Tables 2** and **3**.

The rock mass deformation modulus was calculated using standard empirical equations (Khanlari et al., 2012; Shen et al., 2012). The effect of disturbance on rock mass properties for the sections of the Golab tunnel excavated by drilling and blasting was also considered (Sections 3 and 8) (Rockscience, 2007). The rock mass deformation modulus was calculated by averaging the values estimated by different empirical equations to decrease the error because each empirical equation depends on some rock mass properties (Khanlari et al., 2012).

Table 2: The geotechnical sections along the Golab tunnel, including the geological properties (Zayandab, 2006)

Section	Chainage (m)	Lithology	*Q*	*GSI*	Geological unit
1	0-1210	Conglomerate	5.1-23	66-73	E^{c}
2	1210-1550	Limy shale	2-6.7	66-70	K_4^{lsh}
3	1550-2730	Siltstone & shale	0.3-1.25	57-67	$K_4^{sh,s}$
4	2730- 3050	Shale	0.7-5.7	62-74	K_4^{sh}
5	3050-6570	Limy shale	7.8-23.7	65-77	K_4^{lsh}
6	6570-6800	Shale	0.55-0.83	63-68	K_4^{sh}
7	6800-8100	Limy shale	5.2-15.8	69-80	K_4^{lsh}
8	8100-8570	Shale	0.25-0.5	55-65	K_4^{sh}
9	8570-8800	Limy shale	0.88-1.3	63-68	K_4^{lsh}

359 **Table 3:** The geological properties of the Beheshtabad tunnel (Zayandab, 2010)

Section	Chainage (m)	Lithology	*Q*	*GSI*	Geological unit
1	7600-8120	Marlstone	2.1-4.2	67-76	M_r^m
2	8120-9630	Limestone	7.42-14.8	72-79	OM_a^L
3	9630-10790	Marlstone	1.8-3.6	67-76	M_r^m
4	10790-11100	Sandstone	4.2-12.5	65-69	$PL\text{-}Q_b^s$
5	11100-12110	Conglomerate	9.4-16.5	67-71	$PL\text{-}Q_b^c$
6	12110-15360	Mudstone	1.9-5.8	56-65	$PL\text{-}Q_b^{ms}$

7	15360-16000	Conglomerate & mudstone	0.99-4	56-63	PL-Q_b^c, Q_b^{ms}

Considering the intact rock properties as an upper limit and using the standard deviation values, the estimated values of rock mass characteristics were obtained close to actual values. The properties of intact rock and rock joints and the in-field observations were used to calculate the rock mass parameters, e.g., cohesion strength and internal friction angle (using RocLab software) (Rockscience, 2007).

The study sites (the 0-8.8 km chainage of the Golab tunnel and the 7.6-16 km chainage of the Behesht-abad tunnel) were divided into sections based on lithology, structural features, overburden, and geotechnical characteristics. **Tables** 4 and 5 summarize the range and average value for all parameters.

Table 4: The geotechnical characteristics of the Golab tunnel (0-8.8 km) (Zayandab, 2006)

Section	Intact (Saturated)				Rock Mass				
	σ_{ci}[MPa]	m_i	E_i[GPa]	ν	C[MPa]	ϕ[°]	E_{rm}[GPa]	σ_{cm}[MPa]	ν_{rm}
1	69-86 (77)	21	12.3-24 (19.2)	0.15	2.7-3.6	50.6-53.7	10.9-14.6 (12.7)	11.6-26.6 (19.1)	0.16-0.17
2	34-41 (37.4)	7	12-12.3 (12.1)	0.28	1.4-1.78	38.7-50	6.6-6.8 (6.7)	6.3-11.7 (9)	0.31
3	10-20 (15)	10	7.5-10 (8.7)	0.35	0.64-1.07	30.6-38.7	4.5-4.7 (4.6)	1.9-4.3 (3.1)	0.39-0.4
4	8.7-27 (18.7)	6	9-10.4 (9.7)	0.34	0.54-1.49	27.6-38.6	5-5.8 (5.4)	2.9-8.4 (5.6)	0.37-0.38
5	35-70 (54)	7	14-27 (21)	0.28	1.25-3.6	40-46.3	10.5-17.3 (13.9)	9.2-21.2 (15.2)	0.3-0.31

Section	Intact (Saturated)				Rock Mass				
	σ_{ci}[MPa]	m_i	E_i[GPa]	v	C[MPa]	ϕ[°]	E_{rm}[GPa]	σ_{cm}[MPa]	v_{rm}
6	5-13 (8)	6	2.5-8 (3.6)	0.32	0.35-0.64	26.8-35.1	1.7-4.8 (3.3)	2.4-1.75 (2.1)	0.35-0.36
7	37-69 (58)	7	12-20.7 (17.1)	0.25	1.3-4	31.5-48.5	8-13.6 (10.8)	11.1-22 (16.5)	0.26-0.27
8	5-13 (8)	6	2.5-8 (3.6)	0.32	0.32-0.63	28.8-37	1.3-4.4 (2.9)	2-2.1 (2.05)	0.35-0.36
9	8-22 (13)	7	4-11 (7.5)	0.29	0.4-0.83	33.1-41.8	3.2-6.3 (4.8)	2.3-5.1 (3.7)	0.32-0.33

368 **Table 5:** The geotechnical properties of the host rock along the Beheshtabad tunnel (7.6-16 km) (Zayandab,
369 2010)

Section	Intact (Saturated)				Rock Mass				
	σ_{ci}[MPa]	m_i	E_i[GPa]	v	C[MPa]	ϕ[°]	E_{rm}[GPa]	σ_{cm}[MPa]	v_{rm}
1	9-49 (30)	7	1-5 (3)	0.27	1.3-1.6	35.7-37.4	0.9-1.7 (1.3)	4.9-9.75 (7.3)	0.29-0.3
2	22-81 (59)	10	8-39 (18)	0.24	1.5-1.6	43.6-44.1	9.8-10.2 (10)	10.8-17.4 (14.1)	0.25-0.26
3	9-49 (21)	7	1-5 (2)	0.27	0.94-1.1	33.6-35.4	0.8-1.1 (0.95)	5-7 (6)	0.29-0.3

Section	Intact (Saturated)				Rock Mass				
	σ_{ci}[MPa]	m_i	E_i[GPa]	v	C[MPa]	ϕ[°]	E_{rm}[GPa]	σ_{cm}[MPa]	v_{rm}
4	42-88 (46)	17	8-18 (14)	0.23	1.8-2	47.8-48.8	(7.7)	9.4-15.4 (12.4)	0.25-0.26
5	20-84 (54)	21	8-18 (15)	0.25	2.3-2.5	50.2-51.1	8.8-8.9 (8.85)	13.7-20.3 (17)	0.27-0.28
6	20-52 (37)	6	1-9.5 (4)	0.28	1.2-1.3	35.3-36	1.4-1.6 (1.5)	6-10.2 (8.1)	0.32
7	20-52 (33)	6	1-7.8 (3)	0.28	1.2-1.4	31.6-33.2	0.6-1.2 (0.9)	4.4-9.3 (6.8)	0.31-0.32

2.4. Squeezing prediction

In this section, the observed intensity of squeezing along the Golab tunnel during excavation was related to *ER* values. A relationship was defined between *ER* and the measured normalized strains (based on in-situ data collected by extensometers). Finally, a new strain-based classification system was developed. Throughout this text, N, L, M, S, and VS depict non-squeezing, light, moderate, severe, and very severe squeezing.

2.4.1. Combining numerical modeling and semi-empirical approach

Incorporating simple numerical modeling into a semi-empirical approach was previously considered an option to predict tunnel squeezing (Khanlari et al., 2012). The possibility of instability and support problems can be higher when tangential strain at the tunnel periphery passes the critical threshold (Aydan et al., 1993). The Aydan method (**equation 1**) can be linked to numerical modeling to calculate rock deformations around a tunnel. The squeezing index can be calculated as the ratio of calculated to critical strain:

$$SI=\frac{u_a/a}{\varepsilon_{cr}} \quad (1)$$

For SI<1, tunnel squeezing is impossible; for 1<*SI*<2, L; for 2<*SI*<3, M; for 3<*SI* <5, S; and *SI* >5, VS (Aydan et al., 1996). The critical strain can be calculated by experiment-based relations, such as **Equation 2** (Singh et al., 1997) and **Equation 3** (Barton, 2002):

$$\varepsilon_{cr}=31.1\frac{\sigma_{ci}^{1.6}}{E_i\gamma^{0.6}Q^{0.2}} \quad (2)$$

$$\varepsilon_{cr}=5.84\frac{\sigma_{ci}^{0.88}}{Q^{0.12}E_i^{0.63}} \quad (3)$$

Numerical modeling was used to evaluate the normalized radial closure, u_a/a; the finite difference program FLAC^{2D} (ITASCA, 2002) was used to calculate strain values. Input parameters were residual stress, dilation angle, and residual strength properties of the rock masses. Because the overburden of tunnels was high, the dilation angle can be considered zero (Mair et al., 2002).

With an assumption of the ideal elastic-plastic rock behavior, the residual strength parameters were set similarly to the peak values. Therefore, the rock mass characteristics, including the deformation modulus, poison ratio, cohesion, and internal friction angle (i.e., the outputs of RocLab), were incorporated in FLAC^{2D}. For the stress state, vertical in-situ stress (γz) was applied. The horizontal stresses were calculated based on multiplying *K* values (the ratio of horizontal to vertical stress, i.e., **equations 4** and **5**) by γz. Maximum and minimum stress coefficients were determined by the following equations (Khanlari et al., 2012):

$$K_H=0.98+\frac{250}{z} \quad (4)$$

$$K_h=0.65+\frac{150}{z} \quad (5)$$

In the numerical models, the horizontal fixed boundary condition was considered at the left and right sides of the domain, and the XY-fixed boundary was imposed on the bottom model boundary. Several models were simulated to evaluate the optimum distance from the excavation boundary to avoid boundary effects. This distance was calculated as ten times the tunnel diameter.

Each model side was considered 100 m based on several runs of numerical modeling. In each direction, 100 grids were set; a finer mesh size was used close to the tunnel periphery. After reaching the initial equilibrium (i.e., in-situ stress condition), the excavation was simulated. Then, the support system was installed.

The support system was installed at a distance from the excavation face (by permitting a certain amount of deformation before installing the support) (Rocscience, 2004).

The evaluated closure values were implemented in the semi-empirical equation (Aydan et al., 1996), and the squeezing was predicted based on the calculated *SI* values. This method (the Aydan-FDM) combined simplified numerical modeling and semi-empirical methods (**Figure** 7). We compared the results of this method to real squeezing cases along the Golab tunnel to determine its accuracy compared to the production-phase data.

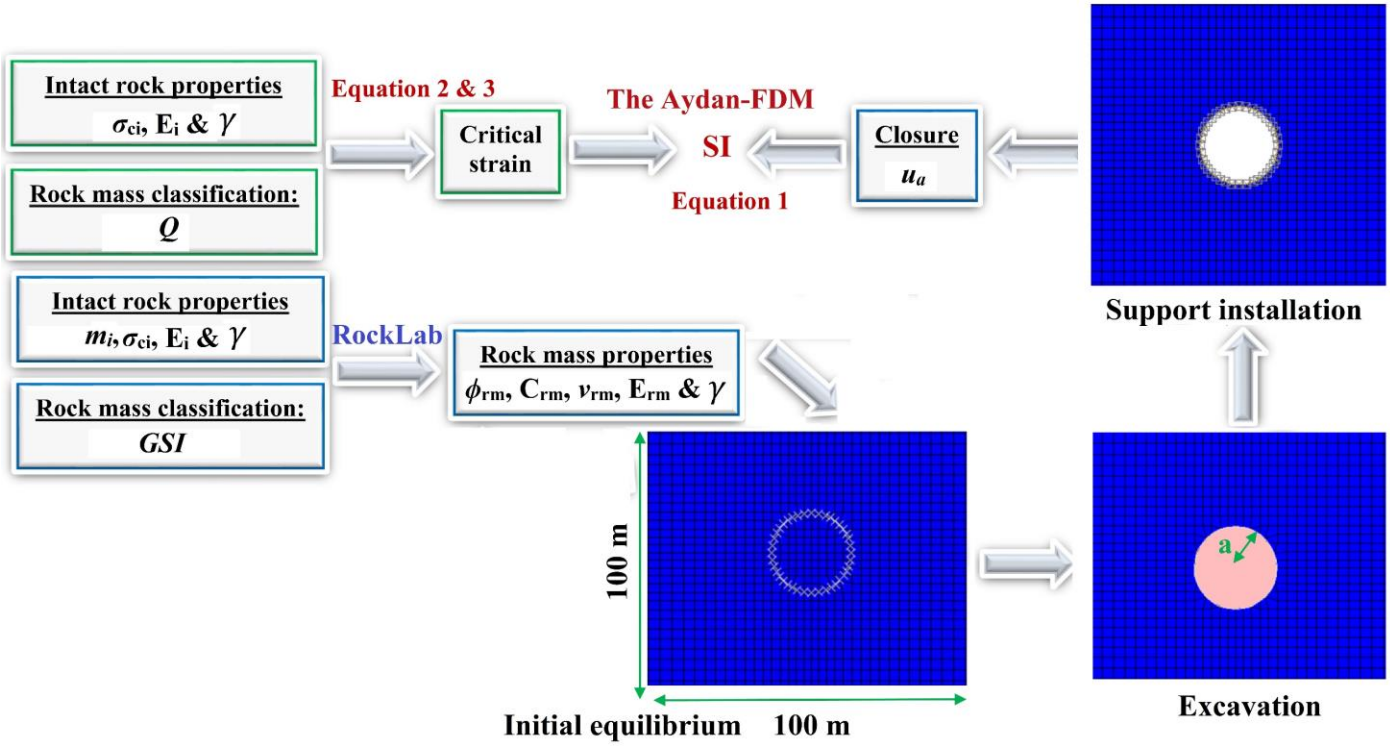

Figure 7: The flow chart of the Aydan-FDM for predicting squeezing.

2.4.2. Electrical resistivity and observations

A comprehensive data set was available for time-dependent deformations, support failures, financial costs, and rock mass conditions for the excavated Golab tunnel. The rock and stability conditions of the Golab tunnel were compared with the frequently-used qualitative classification of tunnel squeezing (Aydan et al., 1993; Palmstrom, 1996; Hoek & Marinos, 2000), and the squeezing intensity was defined along the tunnel length. The main drawback of predicting squeezing with this approach was the qualitative presentation

of the squeezing. Previous semi-empirical equations were also developed based on site-specific data and some, not all, geotechnical properties.

The normalized tunnel strain (ε) can be considered the only quantitative parameter to classify squeezing. However, using this parameter can be problematic: (1) calculating ε based on empirical equations or numerical models, e.g., (u_d/a) in the Aydan-FDM introduced in **section 2.4.1**, can cause an error. (2) for accurate measurement of ε, we required the recorded deformations during or after the excavation. However, the objective of this research work (similar to many other projects) was to predict squeezing in the design phase.

Correlating ε and another parameter with two intrinsic properties was the aim of this work. Such a parameter should be related to tunnel squeezing and can be measured before excavating the tunnel. *ER* was chosen as the parameter satisfying these two requirements, which can indirectly predict time-dependent behavior, based on what was mentioned in the Introduction section.

Calibrated *ER* values were related to the qualitative squeezing classification along the Golab tunnel. Then, an *ER* range was considered for each squeezing intensity class. Since the in-situ closure data of the Golab tunnel was recorded during the excavation by a convergence tape (Moosavi & Khazaei, 2003), accurate values of ε were measured at 60 sections. In each part, five pins were installed to measure the displacements with an accuracy of 0.01 mm (Zayandab, 2006). Therefore, we related *ER* to the in-situ values of ε. The ε-*ER* chart was prepared based on the recorded in-situ data. Finally, the effects of various parameters on squeezing intensity were evaluated using the newly developed approach. The squeezing prediction based on the *ER* is summarized in **Figure 8**.

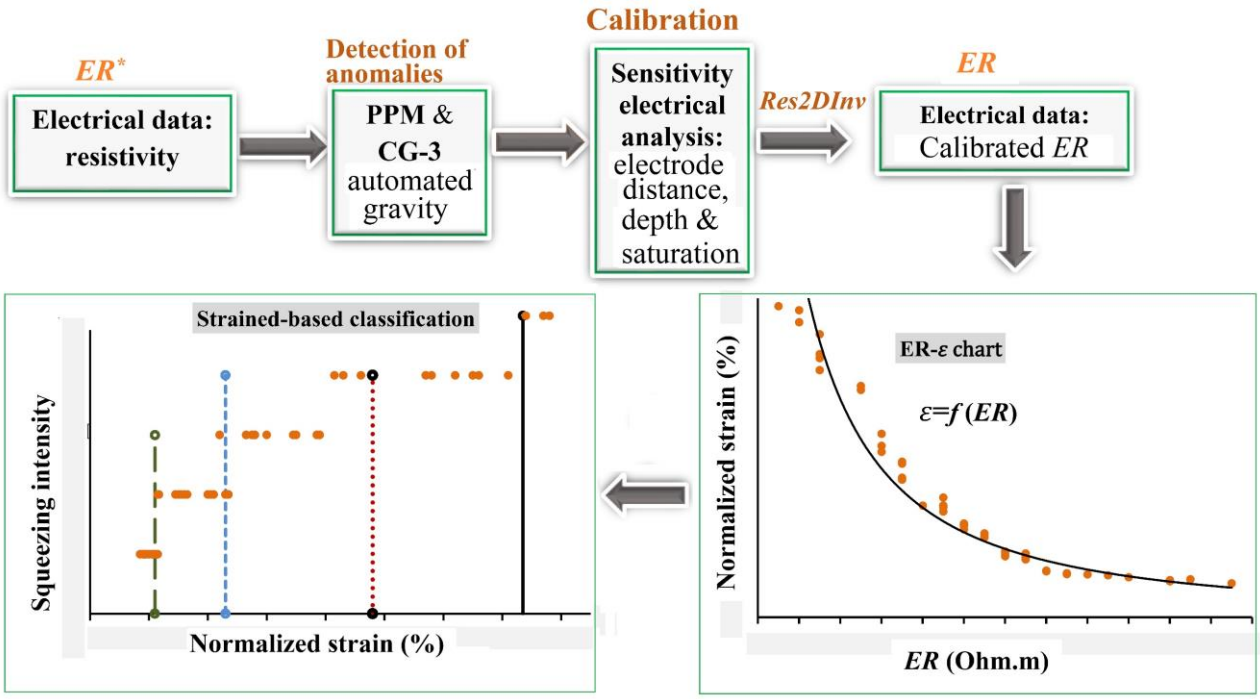

Figure 8: The flow chart for predicting squeezing based on geoelectrical data and the in-situ strains

The steps in **Figure 8**, except the last one (the strain-based classification), are related to the data of the Golab Tunnel used for calibration. Then, the normalized strain-squeezing intensity was used to predict the squeezing of the Beheshtabad Tunnel. The quantitative approach was used to predict squeezing for various conditions of the rock type, depth, saturation, and joint properties.

3. Results

The in-situ stress state of the study sites was evaluated by **equations 4** and **5** (**Tables 6** and **7**). The strength parameters of some rock masses were lower (**Tables 2–4**) compared to the Golab tunnel; therefore, the squeezing problem can be more plausible along the Beheshtabad tunnel.

We considered the average values of **equations 2** and **3** as the critical strain in each section (**Table 8**). Each value was evaluated as a range because we defined a range of intact rock properties based on laboratory experiments. The values of $\frac{u_a}{a}$ (calculated by $FLAC^{2D}$) were divided by the average value of ε_{cr} (**Table 8**). **Figure 9** shows displacement contours for Section 8 of the Golab tunnel in a 20 m×20 m plot window. The values in **Table 8** were incorporated into Aydan et al. (1996) semi-empirical equation to predict the squeezing intensity (the Aydan-FDM).

Table 6: The stress components along the sections of the Golab tunnel

Section	Chainage (m)	ρ [kg/m^3]	Z [m]	σ_v [MPa]	K Values			σ [MPa]	
					K_h	K_H	K_{Hh}	σ_h	σ_H
1	0-1210	2700	450	11.92	0.98	1.54	1.26	18.3	11.72
2	1210-1550	2750	290	7.68	1.17	1.84	1.51	14.15	8.97
3	1550-2730	2640	270	6.99	1.21	1.91	1.56	13.33	8.43
4	2730-3050	2740	240	6.45	1.28	2.02	1.65	13.04	8.23
5	3050-6570	2750	200	5.40	1.4	2.23	1.82	12.03	7.55
6	6570-6800	2750	160	4.32	1.59	2.54	2.06	10.97	6.85
7	6800-8100	2760	145	3.93	1.68	2.7	2.19	10.62	6.61
8	8100-8570	2730	130	3.48	1.8	2.9	2.35	10.11	6.28
9	8570-8800	2750	120	3.24	1.9	3.06	2.49	9.92	6.15

Table 7: The stress components of the sections along the Beheshtabad study site

Section	Chainage (m)	ρ [kg/m^3]	Z [m]	σ_v [MPa]	K Values			σ [MPa]	
					K_h	K_H	K_{Hh}	σ_h	σ_H
1	7600-8120	2500	360	8.83	1.07	1.67	1.37	9.42	14.78
2	8120-9630	2680	305	8.02	1.14	1.80	1.47	9.16	14.43
3	9630-10790	2680	300	7.89	1.15	1.81	1.48	9.07	14.30
4	10790-11100	2600	320	8.16	1.12	1.76	1.44	9.13	14.38
5	11100-12110	2700	370	9.80	1.06	1.66	1.36	10.34	16.23

6	12110-15360	2610	330	8.45	1.10	1.74	1.42	9.33	14.68
7	15360-16000	2650	430	11.39	1	1.56	1.28	11.38	17.78

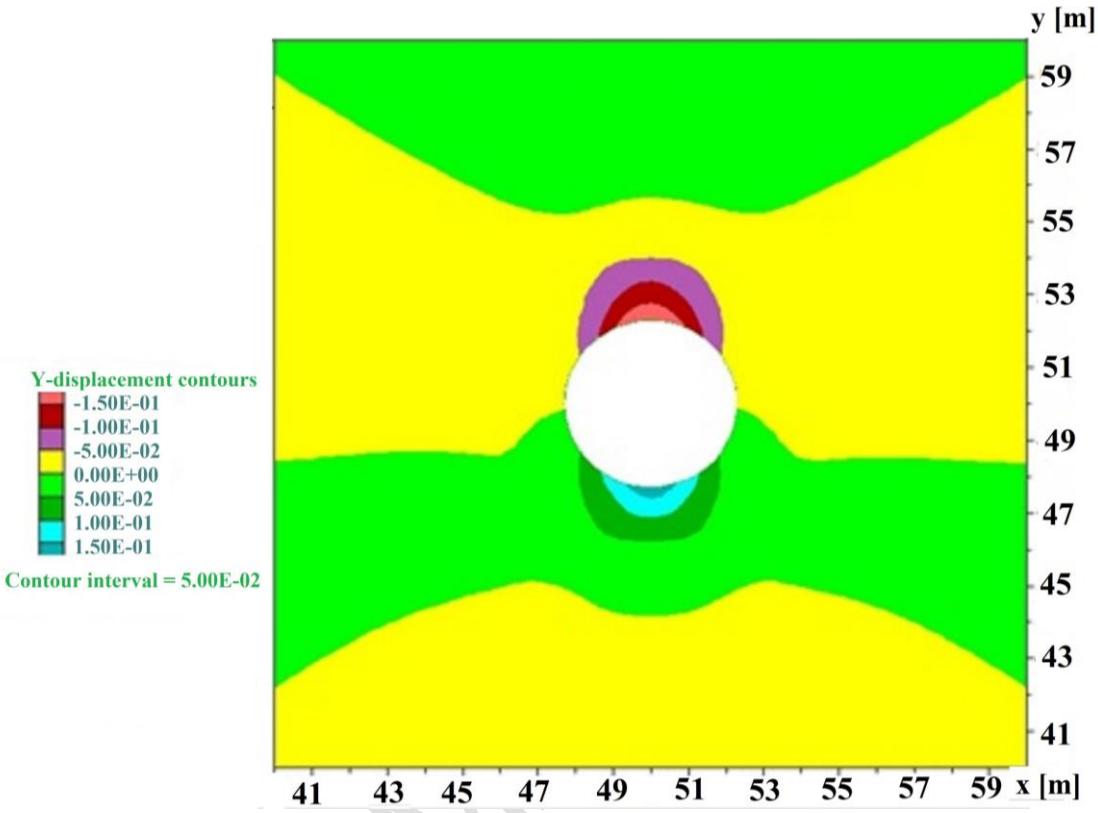

Figure 9: Displacement contours of Section 8 of the Golab tunnel by the numerical modeling, FLAC^{2D} (40 < x < 60 m; 40 < y < 60 m). The unit of the Y-displacement contours is a meter (ITASCA, 2002).

Table 8 lists the in-situ measured strains. A ε range was also presented because several measurements were recorded along each section of the Golab tunnel. The difference between in-situ ε and $\frac{u_a}{a}$ can illustrate the accuracy of the numerical modeling, i.e., the Aydan-FDM.

Table 8: The critical strain, calculated, and measured ε along the Golab tunnel

	Critical strain (%)				
Section	**Calculated by equation 2**	**Calculated by equation 3**	**Average value**	**u_a/a [%]**	**ε [%]**

1	0.5-0.67	0.37-0.44	0.47	0.22	0.85-2.3
2	0.32-0.4	0.3-0.35	0.33	0.4	1.1-2.35
3	0.15-0.19	0.2-0.24	0.19	1.16	2.8-7.8
4	0.13-0.2	0.19-0.25	0.18	1.65	1.17-3.85
5	0.25-0.32	0.25-0.29	0.27	0.23	1.07-3.45
6	0.14-0.15	0.21-0.22	0.18	7.47	2.35-2.8
7	0.38-0.44	0.32-0.35	0.37	0.11	1.6-6.5
8	0.13-0.15	0.21-0.23	0.18	8.19	3-6.6
9	0.13-0.14	0.2-0.21	0.17	1.86	1.5-1.53

The qualitative classification based on previous studies (Aydan et al., 1993; Palmstrom, 1996; Hoek & Marinos, 2000) is shown in **Table 9**. This classification was used to determine the squeezing intensity along the Golab tunnel, and the range of *ER* values of the tunnel was recorded for each intensity class.

Table 9: The qualitative classification of squeezing for soft sedimentary rocks at the Golab study site

Squeezing (Observed)	**Rock characteristics (Aydan et al., 1993; Palmström, 1996; Hoek & Marinos, 2000)**		***ER*** **[Ohm.m]**
	Rock behavior	**Stability condition**	
No squeezing	Elastic	Stable tunnel as face effects is terminated	170-270
Light	Strain-hardening	Stable tunnel and converged displacement as face effects are stopped	120-180

Moderate	Strain-hardening	Large displacement: converged displacement after face influence	80-130
Severe	High strain-hardening	Extreme displacement: not converge when face effects stop	60-90
Very severe	Rock flow and collapses	Extreme displacement: re-excavation & heavy support are required.	<60

Table 10 shows calibrated electrical values for each section and the variation of squeezing conditions along the Golab tunnel. The squeezing intensity based on the *ER* and Aydan-modified approaches is also presented. At the *GSI* range of 60-70, the *ER* of saturated siltstone (the green bar) and conglomerate (the red bar) was decreased from 150 to 60 and 220 to 190 Ohm.m, respectively (**Figure 10a**).

The decrease of *ER* due to the water saturation, under constant *GSI* (**Figure 10a**), was higher for the rocks with higher amounts of clay, e.g., 60 % and 41 % for siltstone and shale, while 13.6 % and 20 % for the conglomerate and limy shale. At approximately constant depth, the effects of rock mass condition (or *GSI*) on the *ER* of the saturated tocks (**Figure 10b**) were also noticeable. The resistivity decreases from 23.5 (for conglomerate) to 62.5 % (for limy shale).

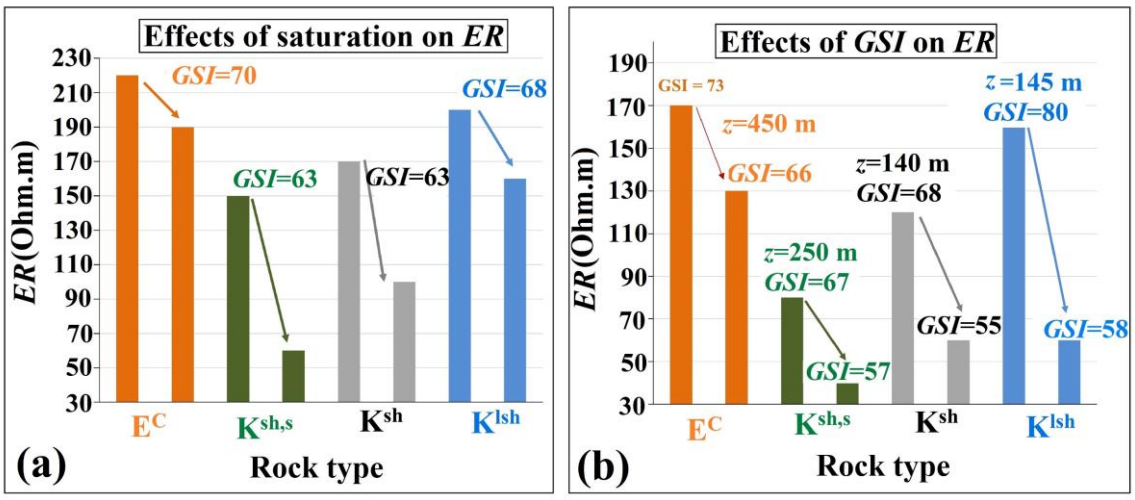

Figure 10: Results based on sensitivity electrical analysis of calibrated geoelectrical data for the Golab tunnel: (a) Effects of water saturation on the electrical resistivity of the rocks under constant GSI (fracture condition)

and depth difference of < 30 m. (b) Effects of GSI alterations on the electrical resistivity of the saturated rocks under relatively constant depth (*z*).

Figure 11 shows the occurrence of stability issues along some sections of the Golab tunnel. The squeezing problems based on the *ER* and Aydan-modified are presented in **Table 11**. The observed squeezing cases and *ER* variations are shown (**Figure 12**) from 0 to 3.25 km along the Golab tunnel.

Table 10: Squeezing intensity along the Golab tunnel based on electrical resistivity, Aydan-FDM, and the field observations: N, L, M, S, and VS depict non-squeezing, light, moderate, severe, and very severe squeezing, respectively.

Section	Aydan-FDM		Field observations (Table 8)	*ER* [Ohm.m]
	SI	Squeezing class		
1	0.5	N	N-L	130-260
2	1.2	L	N-M	120-220
3	6.1	VS	M-VS	50-110
4	9.2	VS	L-M	90-170
5	0.9	N	N-M	90-190
6	41.5	VS	N-M	110-160
7	0.3	N	L-M	90-160
8	45.5	VS	M-S	60-120
9	10.9	VS	L	120-160

Table 11: The total length of each squeezing class and prediction errors of the *ER*-based and Aydan-FDM approaches for the Golab tunnel

Squeezing class	Chainage (for intensity classes) (km)		Prediction errors (%)	
	Aydan-FDM	*ER*	Aydan-FDM	*ER*
No	6.03	1.1	445	0.1
Light	0.34	1.1	93.6	2.83
Moderate	0	5.45	100	5.7
Severe	0	1.84	100	2.43
Very severe	2.43	0.75	548	1.4

Based on the field observations, the length of N, L, M, S, and VS squeezing conditions was 1.105, 5.305, 1.745, 0.74, and 0.375 km, respectively. The squeezing calculated based on the Aydan-FDM was evaluated for each squeezing class. The total length of sections predicted with N, L, M, S, and VS conditions was 6.03, 0.34, 0, 0, and 2.43 km, respectively. Therefore, the Aydan-FDM predicted the squeezing with an average error larger than 100 %.

The prediction accuracy of the Aydan-FDM may vary for other formations as it was developed based on the accuracy of geotechnical parameters at the study site. For the *ER*-based approach, some sections were divided into several squeezing classes. e.g., for Section 2 of the Golab tunnel, chainages 1210-1319, 1319-1495, and 1495-1550 m were detected as no, light, and moderate squeezing classes, respectively. According to the foreseen lengths for intensity, the accuracy of geoelectrical prospecting along the Golab tunnel was at least 94 %. Therefore, the qualitative classification based on geoelectrical mapping was more accurate than the Aydan-FDM, and squeezing can be evaluated accurately in a section, not in a location. Hence, we developed the relationship between the in-situ measured strains and *ER* and prepared the new classification system based on ε. This methodology provided a quantitative relationship for predicting squeezing (**Equation 6**).

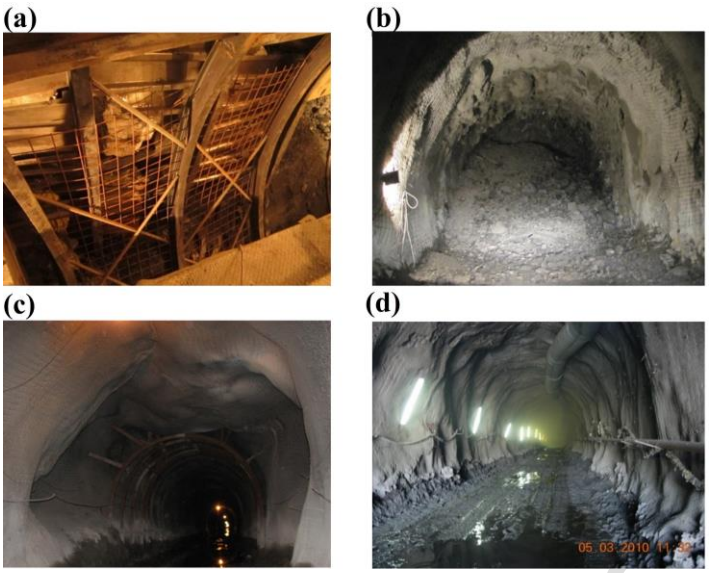

Figure 11: The stability problems related to squeezing observed along the Golab study site: (a) Section 1 (322 m from the inlet): light deformations, (b) Section 2 (1550 m): severe deformations and rock flow, (c) Section 3 (2961 m): moderate deformations and collapse of the crown, (d) Section 4 (2987 m): light deformations.

Figure 13a presents a chart based on the relationship of the in-situ measured strains (**Table 8**) and *ER*, and a new strain-based classification system was introduced for predicting ε (and consequently squeezing) based on *ER* (**equation 6**). In the next stage, for each squeezing class, the *ER*-ε relationship was used to calculate the strain range based on *ER* (**Table 12** and **Figure 13b**). The step-wise shape of **Figure 13b** was unrelated to the correlation between data, and it depicts the range of predicted normalized strain for each squeezing class in the collected data of this study.

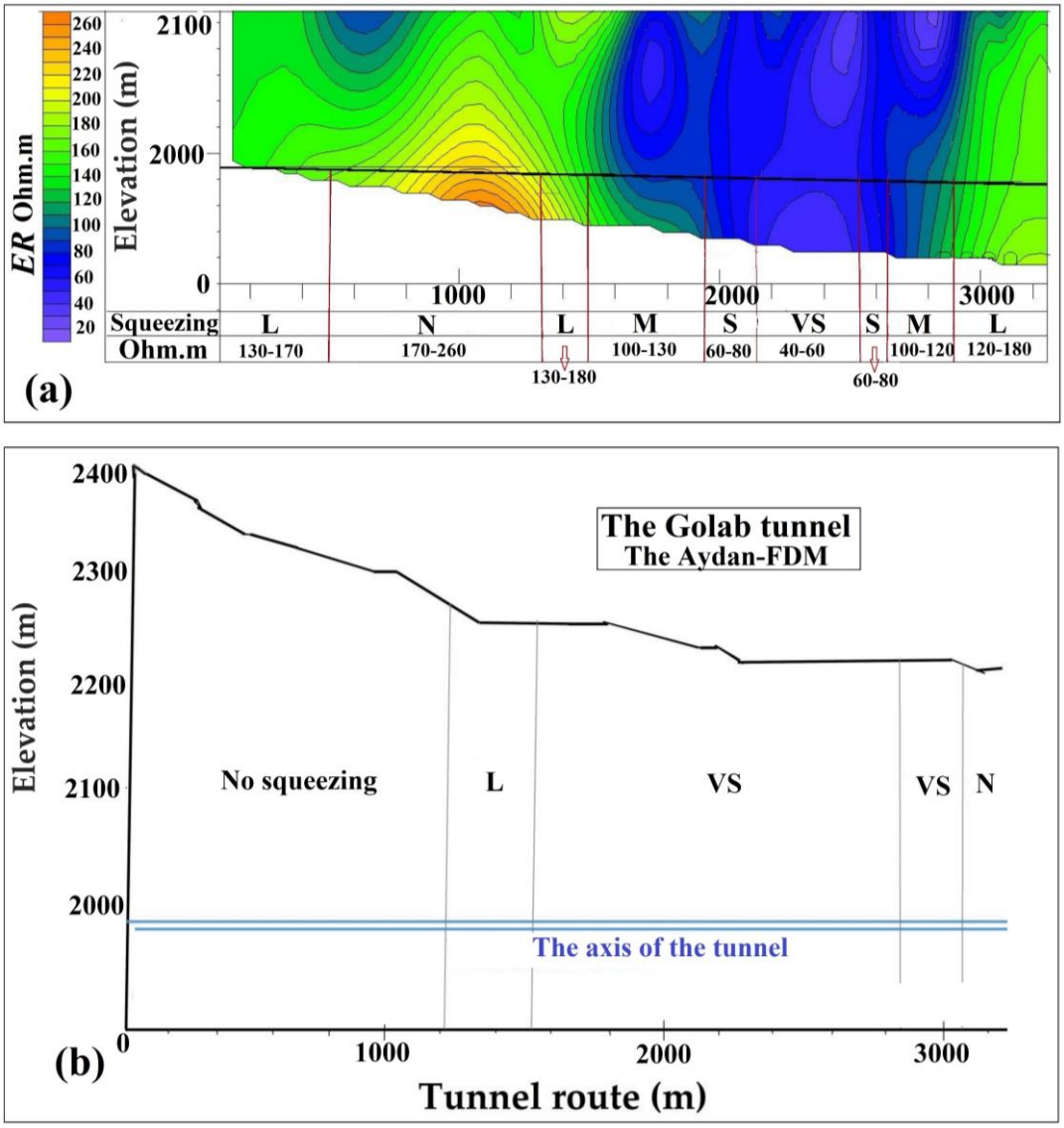

Figure 12: The squeezing predicted based on (a) *ER* and (b) the Aydan-FDM (0-3250 m of the Golab tunnel)

This new approach (**equation 6**) provided quantitative results for predicting squeezing based on the strains calculated by *ER* values. The accuracy of the new classification system was 89.14 %, considering the *R-square* value of the *ER-ε* chart and the prediction error of the resistivity approach, 94 %.

$$\varepsilon[\%] = 3538\ ER^{-1.523} \quad 30 < ER\ [\text{Ohm.m}] < 270 \qquad \textbf{(6)}$$

Table 12: The new classification system of the squeezing intensity by the measured strains along the Golab tunnel (**Equation 6**)

Squeezing intensity	No squeezing	Light	Moderate	Severe	Very severe
Normalized strain (%)	$\varepsilon \leq 1.1$	$1.1 < \varepsilon \leq 2.3$	$2.3 < \varepsilon \leq 4.8$	$4.8 < \varepsilon \leq 7.35$	$\varepsilon > 7.35$

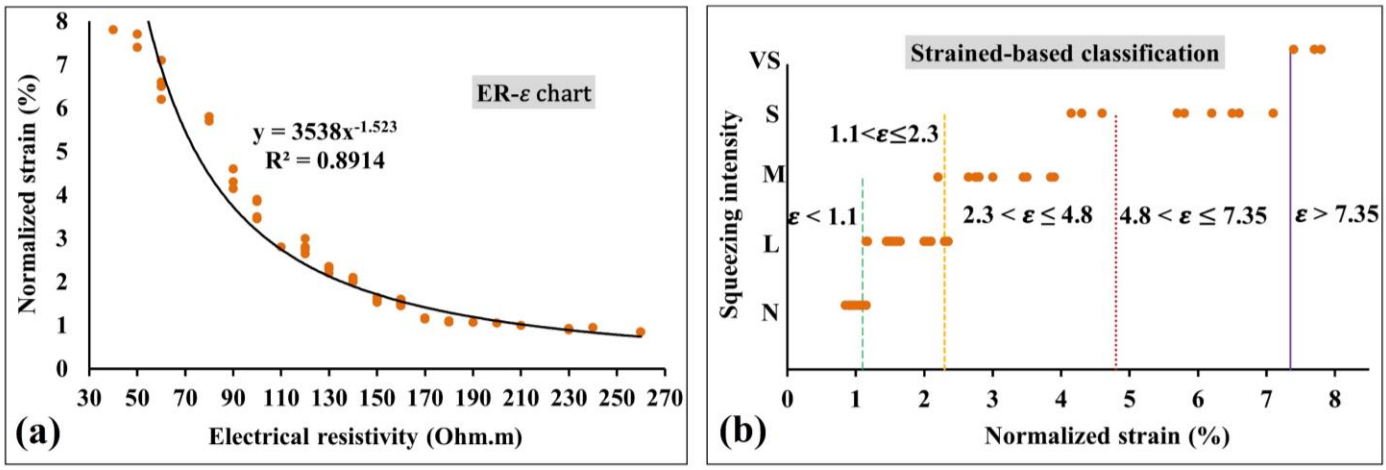

Figure 13. (a) The relationship between the ε (measured in 60 locations by the convergence tape) and *ER* (based on **Table 8**). (b) The strain ranges for each squeezing class. The data are related to the Golab tunnel after excavation. N, L, M, S, and VS depict No, Light, Moderate, Severe, and Very Severe squeezing conditions.

The squeezing potential along different sections of the Beheshtabad tunnel was predicted (**Table 9**)-presented in **Figure 14a**. The squeezing potential can vary even along a geotechnical section. For instance, the squeezing changed from M to VS class along Section 2. A similar trend was observed during the excavation of the Golab tunnel. Variations of squeezing intensity can be related to the heterogeneity of different geotechnical and geological properties.

Each line in **Figure 14a** shows the range of *ER* along a section of the Beheshtabad tunnel and presents the predicted squeezing intensity based on the geoelectrical qualitative approach. For example, the squeezing was defined as S from 7600 to 8400 m based on two ranges of *ER* (60-90 and 75-90 Ohm.m).

For the comparison analysis, the predictive values of the Aydan-FDM are also presented in **Figure 14b**. The predicted length of M, S, and VS squeezing classes based on *ER* approach along the Beheshtabad tunnel was 3425, 2355, and 2620 m, respectively. No zone was predicted as S or L squeezing conditions.

The squeezing intensity along the Beheshtabad study site was also evaluated by **Equation 6** (**Figure 14c**). Variations in **Figure 14 a, c** was related to the fact that a range of *ER* or strain was recorded for each squeezing condition along tunnel sections. For example, for the first section (7800-8400 m), *ER* and ε ranged from 60 to 90 Ohm.m and 3 % to 7 %, respectively. However, the squeezing condition was predicted as severe for the whole range.

The step-wise format was related to variations of squeezing intensity along sections of the tunnel and unrelated to the accuracy of the methodology. For example (according to **Figure 14**), in chainage 9200-10000 m, *ER* and ε varied between 45 to 85 Ohm.m and 2.7 to 10.5 %, respectively. The squeezing intensity showed a dramatic rise from M to VS conditions, with some variations of S and VS conditions between 9500 to 10000 m.

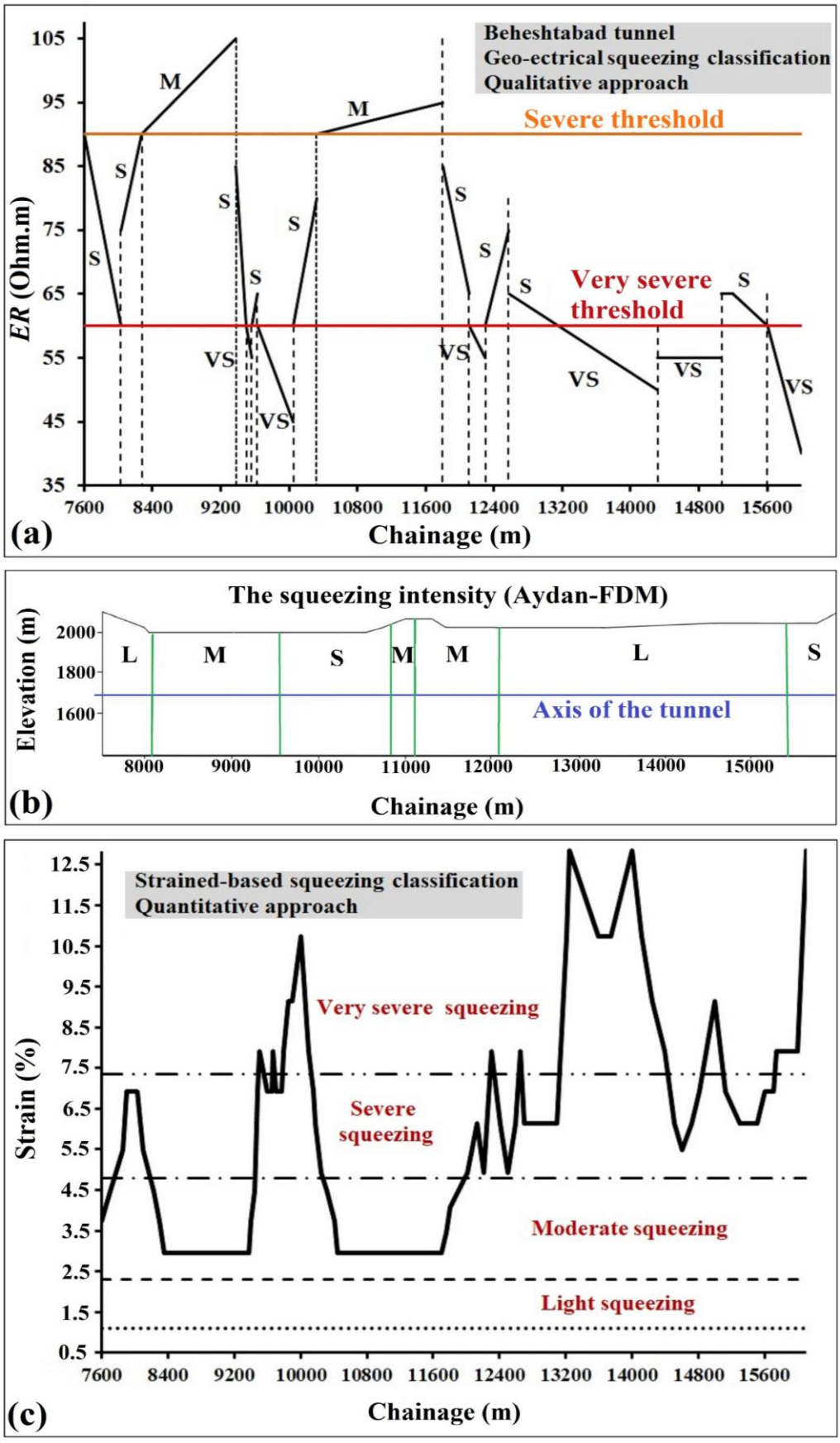

Figure 14: The squeezing intensity along the Beheshtabad site predicted by (a) the qualitative classification based on the variation of the *ER*, (b) the Aydan-FDM, and (c) the quantitative strained-based classification

(**Equation 6**). The saturated rocks at the tunnel depth (axis) were considered. Squeezing classes are defined based on the range of calculated strains (e.g., for 7600 to 8000 m, the intensity increases from M to S along this section).

The relation of *ER* with rock mass indices and rock mass properties along the Golab tunnel is represented in **Figure 15**. We evaluated the effects of these parameters on *ER* using the newly-developed quantitative strained-based system (**Figure 16**). The higher the *Q* and *GSI* values were, the bigger the *ER* value was. Therefore, a direct relationship was confirmed between *ER* and rock mass condition (as predicted).

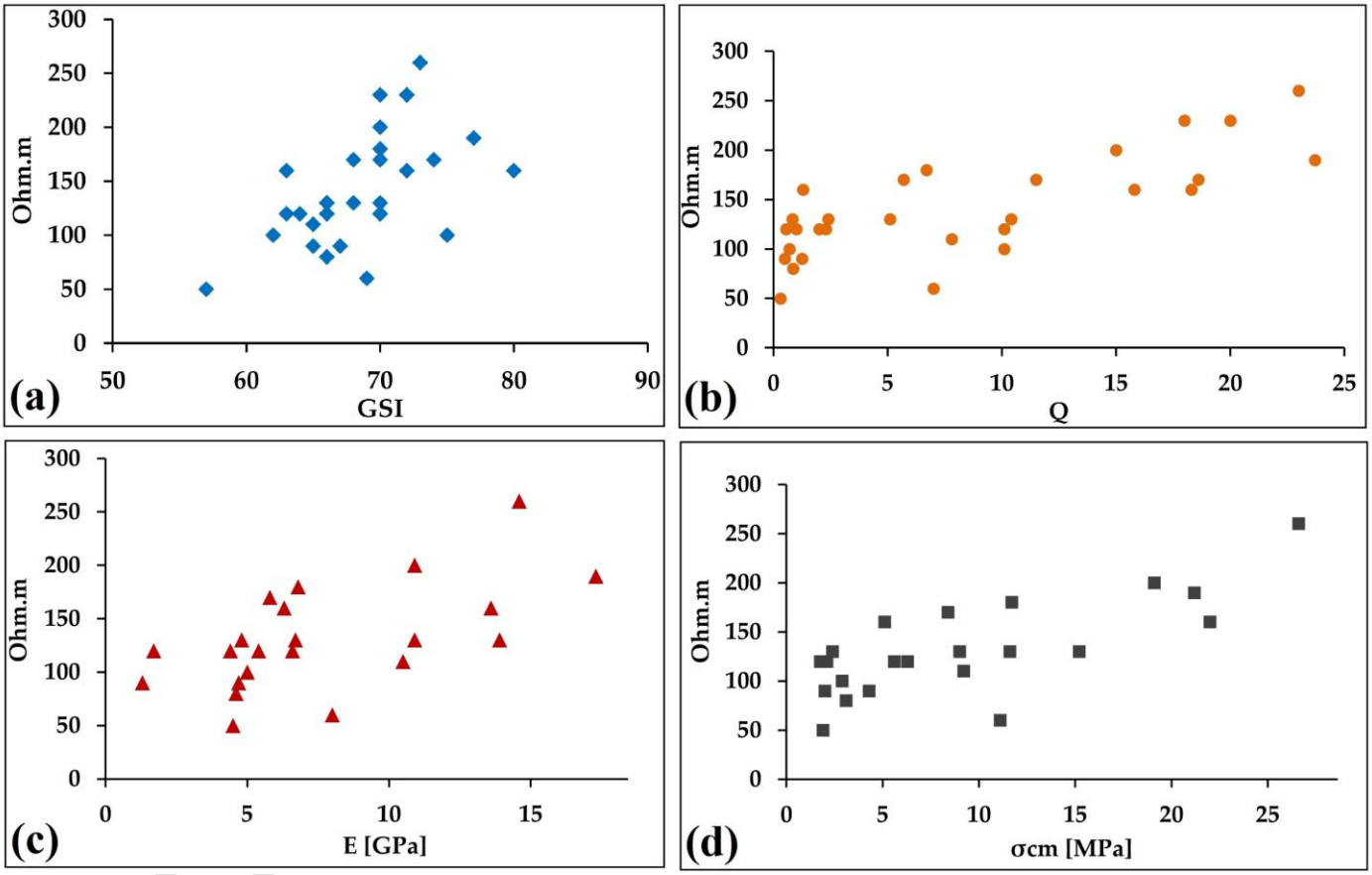

Figure 15. The geoelectrical resistivity versus the rock mass indices and strength parameters for the Golab tunnel for the saturated rocks at the tunnel depth (axis): values were measured after excavation.

In **Figure 16**, the effects of water saturation and *GSI* is shown. The depth was kept almost constant (depth difference < 30 m) while other parameters were compared (without depth effects). Then, the *ER* values recorded in these conditions were used to predict the normalized strain.

The strains increased by about 151 and 187 % for mudstone and marlstone, respectively (for a constant *GSI* value and a depth difference of less than 30 m). The increase was 109 and 114 % for the conglomerate and limestone. Therefore, the squeezing intensity changed: from L to M for conglomerate and limestone, from M to S for mudstone, and from M to VS for marlstone (see **Table 12** and **Figure 16a**).

At an approximate constant depth, the effects of *GSI* on *ER*-based strains of the saturated rocks were also noticeable. The measured ε of mudstone, marlstone, conglomerate, and limestone were increased by about 160, 187, 107, and 167 %, respectively. i.e., the squeezing intensity altered from severe to VS, M to VS, M to S, and M to VS. The maximum strain of saturated marlstone decreased from 10.7 to 6.9 % for a depth increase of 300 to 360 m, while the maximum ε of saturated mudstone remained constant at 12.8 % for depths 330 and 380 m.

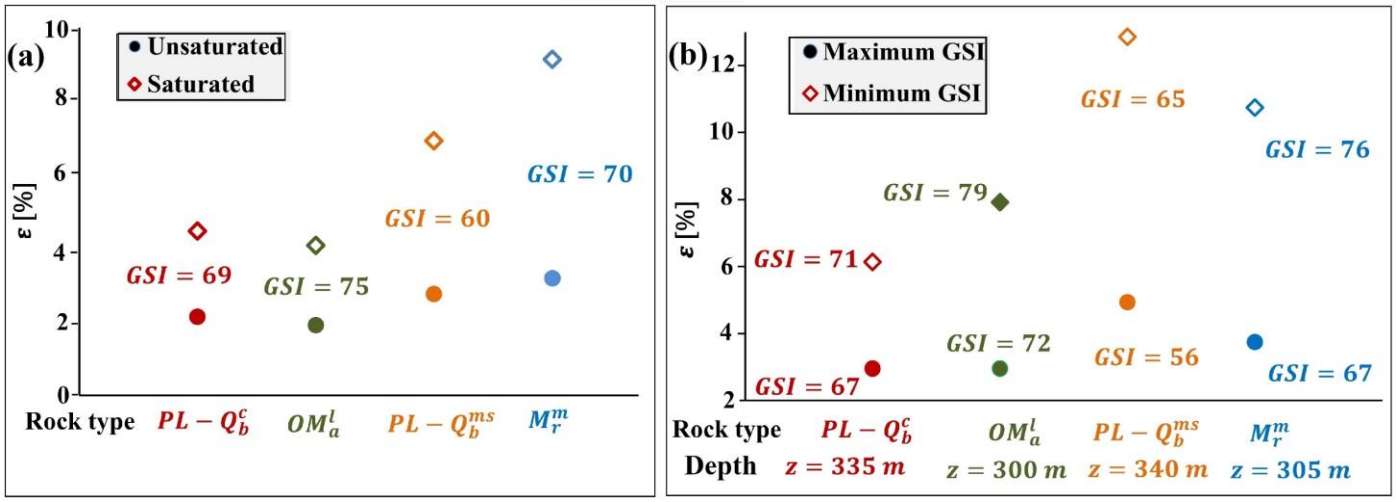

Figure 16. The strain values predicted for the Beheshtabad tunnel by **Equation 6**: (a) the effects of water saturation on the strain of the rocks under constant *GSI* and depth difference < 30 m. (b) The influences of *GSI* on the strain of the saturated rocks. For (b), the depth (*z*) is constant (mentioned below the rock mass type).

4. Discussion

The *ER*-based approach can be a valid hypothesis to predict squeezing at the design phase. Meanwhile, technical measures at the production phase (e.g., installing heavy supports) should be evaluated based on

584 complementary data achieved during the excavation, e.g., coupled three-dimensional numerical models (us-
585 ing more accurate geotechnical data, e.g., in-situ measurements). We indirectly calculated the time-depend-
586 ent rock mass deformations similar to the conventional approaches of predicting squeezing. The difference
587 was related to using *ER* instead of classification systems or empirical equations. This assumption can result
588 in more accurate outcomes for the design phase.

589 The advantages of predicting squeezing based on *ER* can be (1) geophysical methods are fast, non-
590 destructive, and environmentally friendly. (2) Geophysical set-ups, e.g., the number of electrodes, are adapt-
591 able to cover the whole study area. Therefore, the final results are based on large-scale data compared to the
592 limited geotechnical data gathered from boreholes/galleries. (3) The parameters affecting squeezing, e.g.,
593 the hydraulic and geologic characteristics, can influence *ER* likewise. Including more influential parameters
594 (e.g., joint condition, degree of weathering) can increase the accuracy. (4) Geotechnical sections can be
595 divided into more sub-sections with different squeezing classes, and the accuracy can be higher. The number
596 of subsections for the Aydan-FDM and ER-based methods (**Figure 14a** and **Figure 14b**) was 14 and 6,
597 respectively. (5) Geophysical studies (particularly in large projects) are common and without imposing extra
598 financial costs to the design phase, like performing in-situ tests.

599 All available geotechnical approaches present a universal classification system for all types of squeezing
600 (Aydan et al., 1993; Palmström, 1996; Hoek & Marinos, 2000), including those related to the topographic
601 or tectonic mechanisms. This classifying approach may result in erroneous results. However, the developed
602 strain-based equation can provide more accurate data for squeezing in soft rocks (using the calibrated *ER*
603 values).

604 Many squeezing cases are tectonic-based and can occur at a low depth (Shrestha & Broch, 2008). The
605 predicted squeezing intensity (based on measured strains) was detected unrelated to depth. Some previous
606 works categorized the squeezing only on the overburden (Singh et al., 1992; Goel et al., 1995). The probable
607 reason for this unclear relationship can be the complicated stress state of the study site and factors (such as
608 the stress ratio, tectonic conditions, and fault activations). Tectonic conditions are partially understood and
609 may alter based on findings during the production phase (Guan et al., 2012). Therefore, it can be impossible

to transit these in-field characteristics into a quantified scale, and most previous studies did not consider a tectonic parameter to predict squeezing (Sun et al., 2018). However, detecting fracture zones and faults is one of the main applications of geophysical studies, and tectonic-based squeezing can be predicted at the design phase based on *ER* variations. Dramatic decrease of *ER* due to activation of faults showed that the *ER*-based system predicted tectonic-based squeezing; this ability was visible for the Golab tunnel, e.g., for 0-500 m and 7500-8100 m sections.

A crucial question must be answered: why a significant difference was recorded between the Aydan-FDM and geoelectrical predictive approaches? Several explanations can be presented: (1) The efficiency of the implemented geotechnical data employed in the numerical tool was effective. Determining the rock mass properties based on specific core samples gathered from a few boreholes can cause erroneous results. This uncertainty was crucial in deep tunnels where borehole drilling was a challenging (and costly) task and could not cover large parts of the study area. For example, all geotechnical data of the 7.6-16 km chainage of the Beheshtabad tunnel were evaluated only by four deep boreholes. Therefore, the accuracy of geotechnical input data can impact the numerical model. The considerable difference between calculated $\frac{u_a}{a}$ and measured ε proved the inaccuracy of the numerical results. However, detailed geotechnical studies (e.g., drilling more boreholes or conducting in-situ tests) may provide more accurate geotechnical data and less erroneous squeezing predictions by numerical tools.

(2) The impacts of the geotechnical data on the semi-empirical equations were vital. Improper input parameters can result in poor predictions of the Aydan-FDM (i.e., the ε_{cr} equations were also based on the geotechnical parameters of intact rocks, i.e., limited laboratory experiments). (3) The intentionally simple numerical scheme was used to calculate deformations by FLAC^{2D} because of the limited geotechnical data in the design phase. Some factors (e.g., thermal data or chemical parameters) are rarely measured in the design stage. A fully-coupled numerical model can improve the results; however, running a coupled model specific to the study site is time-consuming. Several three-dimensional models should be built for long tunnels due to the parameter variations. Therefore, in the design phase of many projects, using numerical schemes is limited to simple models. (4) The Aydan equation was developed based on geotechnical data

from tunneling projects in Japan; different site-specific conditions may result in different outputs of this approach.

Despite being more accurate, the main drawback of the *ER* approach was presenting squeezing based on a qualitative explanation (**Table 9**) instead of quantitative data. **Table 9** shows some squeezing classes with shared values of *ER*, e.g., 80 Ohm.m was introduced as a moderate or severe squeezing class. The electrical approach developed in this research cannot also predict the squeezing intensity of hard rocks in deep tunnels. A reason for this incapability was the chosen electrical range (30-270 Ohm.m) in this study; this range was suitable for soft sedimentary rocks. Another limitation was using an almost similar support system for the studied tunnels. Using a heavier support system can affect the squeezing intensity significantly.

Considering the effects of different parameters on the squeezing, alterations of the intensity by mechanical stress (σ_{cm}) were almost invisible (despite increasing). Overburden did not impact squeezing (alterations did not follow a unique trend under variations of depth at a constant *GSI*). The reason can be other factors (such as the stress ratio (*K*), tectonic parameters, and fracture properties).

The squeezing conditions along the Beheshtabad tunnel showed that most parts of the tunnel are prone to severe squeezing, and employing mechanized excavation can be problematic in these zones. Different geological formations in the tunnels, including shale, conglomerate, limestone, siltstone, marlstone, mudstone, and sandstone, were studied for squeezing problems. For both tunnels, high-intensity squeezing was mainly recorded for formations with a high amount of clay, e.g., siltstone and shale at the Golab tunnel. A high decrease of strains (based on *ER*) due to water saturation was visible for the rock masses with high content of clay, i.e., mudstone and marlstone, in the Beheshtabad tunnel.

In the case of complementary studies of predicting squeezing: (1) A more comprehensive database of measured strains (especially from other tunnels excavated in soft sedimentary rocks) can increase the *R-square* value of the *ER*-ε chart and the accuracy of the predictive approach. (2) Other exploration approaches (such as integrated seismic detection) can be combined with geoelectrical data to evaluate tunnel squeezing.

Due to active tectonic structures and high overburden, the stress condition of the Sanandaj-Sirjan zone in Iran is crucial. Regarding the enormous executed/planned tunneling projects in the Central Plateau of Iran, e.g., the Rokh valley water-supply tunnel and Kohrang tunnels, geoelectrical data can predict the squeezing for these projects at the design phase. In the case of deep tunnels excavated in soft rocks, the developed approach predicted the squeezing more efficiently comparing classical methods, although complementary investigations are required.

5. Conclusions

Predicting squeezing at the design stage is a challenging task. Accurate predictive methods can prevent technical difficulties, financial losses, and human injuries during or after the production stage. This study presents the *ER*-based approach to predict squeezing potential along a tunnel. The following conclusions can be highlighted:

- The Aydan-FDM cannot accurately predict rock deformation in soft sedimentary rocks of the Sanandaj-Sirjan zone, maybe due to improper geotechnical parameters or specific conditions of the study sites. The extreme underestimation of squeezing is visible in all sections of the Golab and Beheshtabad tunnels.
- The efficiency of electrical resistivity to predict the squeezing potential is noticeable for soft sedimentary rocks.
- Having a high accuracy in predicting squeezing, the ability to cover a large study area, and being environmentally friendly are all advantages of the *ER*-based method over conventional approaches.
- *ER* is related to the properties of intact rock, fractures, and rock mass. We predict squeezing considering the effects of water saturation, rock type, and joint condition (based on the geoelectrical approach).
- We relate *ER* to in-situ measured strains (a post-excavation parameter). Then, we develop a quantitative strain-based squeezing classification system for tunnels excavated in soft sedimentary rocks.
- The accurate prediction of tectonic-based squeezing is another advantage of the newly-developed method.

- Effects of the rock type, water saturation, and *GSI* on squeezing intensity are noticeable.

Acknowledgments:

We thank the editor and reviewers whose valuable comments and suggestions have led us to improve this manuscript. The authors acknowledge the cooperation with the Zayandab Consulting Engineers Company.

Funding:

M. Akbariforouz is supported by the National Natural Science Foundation of China (No. 41890852), awarded to Chunmiao Zheng. Qi Zhao is supported by the FCE Start-up Fund for New Recruits at the Hong Kong Polytechnic University (P0034042) and the Early Career Scheme of the Research Grants Council of the Hong Kong Special Administrative Region, China (Project No. PolyU 25220021).

Competing Interests:

The authors have no relevant financial or non-financial interests to disclose.

Author Contributions:

Conceptualization, all authors; Data curation, M. A., Q. Zh. and A. B.; Methodology, all authors; Laboratory tests, M. A.; Software, M. A.; Geophysics, M. A.; Validation, all authors; Writing-original draft, M. A.; Writing-review and editing, all authors; Supervision, Ch. B., Q. Zh., and Ch. Zh. All authors have read and agreed to the published version of the manuscript.

References

Aceh, B. (2019). Analysis of Rock Structures Based on Geoelectrical Resistivity Data of Wenner-Alpha Configuration Using Marquardt's s Inversion Method. *Journal of Physics: Conference Series, Volume 1175, 1st International Conference on Advance and Scientific Innovation 23–24 April 2018, Medan, Indonesia*. https://doi.org/10.1088/1742-6596/1175/1/012014

Agan, C. (2015). Prediction of squeezing potential of rock masses around the Suruc Water tunnel. *Bulletin of Engineering Geology and the Environment*. 75, 451–468. https://doi.org/10.1007/s10064-015-0758-1

Akinrinmade, a. O., Ogunsanwo, O., & Ige, O. O. (2013). Geophysical and Geotechnical Investigation of River Ero, Ajuba, Southwestern Nigeria for Dam Development. *International Journal of Science and Technology*, 2(7), 518–528.

Ammar, a. i., Kamal, K. A. (2018). Resistivity method contribution in determining the fault zone and hydro-geophysical characteristics of carbonate aquifer, eastern desert, Egypt. *Applied Water Science, 8(1)*. https://doi.org/10.1007/s13201-017-0639-9

Arora, K., Gutierrez, M., Hedayat, A., & Xia, C. (2020). Tunnels in squeezing clay-rich rocks. *Underground Space (China), XXXX*, 1–14. https://doi.org/10.1016/j.undsp.2020.07.001

Aydan, O., Akagi, T., & Kawamoto, T. (1993). The squeezing potential of rocks around tunnels; Theory and prediction. *Rock Mechanics and Rock Engineering Journal*, *26*(2), 137–163. https://doi.org/10.1007/BF01023620

Aydan, Ö., Akagi, T., & Kawamoto, T. (1996). The squeezing potential of rock around tunnels: Theory and prediction with examples taken from Japan. *Rock Mechanics and Rock Engineering Journal 29 (3)*, 125–143). https://doi.org/10.1007/BF01032650

Backstrom, A. (2004). Investigating fracture frequency and electric resistivity in impact craters in crystalline rocks. *KTH Land and Water Resources Engineering TRI*.

Barla, G., & Barla, M. (2008). Innovative tunneling construction methods in the squeezing rock, *Ingegneria Ferroviaria*, *63*(12), 1017–1031.

Barla, G., Debernardi, D., & Sterpi, D. (2012). Time-Dependent Modeling of Tunnels in Squeezing Conditions. *International Journal of Geomechanics*, *12(6)*, 697–710. https://doi.org/10.1061/(ASCE)gm.1943-

5622.0000163

Barton, N. (2002). Some new Q -value correlations to assist in site characterization and tunnel design. *International Journal of Rock Mechanics & Mining Sciences*, 39, 185–216.

Bernabini, M., Brizzolari, E., & Piro, S. (1988). Improvement of signal-to-noise ratio in resistivity profiles. *Geophysical prospecting*, 36, 559-570.

Bhatt, S., & Jain, P. K. (2014). *C*orrelation between electrical resistivity and water content of sand – a statistical approach. *American International Journal of Research in Science, Technology, Engineering & Mathematics*

Brace, W. F., & Orange, A. S. (1968). Electrical Resistivity Changes in Saturated Rocks during Fracture and Frictional Sliding. Journal of geophysical research, *73*(4), 1433-1445. https://doi.org/10.1029/JB073i004p01433

Chen, G., & Lin, Y. (2004). Stress-strain – electrical resistance effects and associated state equations for uniaxial rock compression. International Journal of Rock Mechanics and Mining Sciences, 41(2), 223–236. https://doi.org/10.1016/S1365-1609(03)00092-3

Chen, Y., Li, T., Zeng, P., Ma, J., Patelli, E., & Edwards, B. (2020). Dynamic and Probabilistic Multiclass Prediction of Tunnel Squeezing Intensity. *Rock Mechanics and Rock Engineering Journal*, *53*(8), 3521–3542. https://doi.org/10.1007/s00603-020-02138-8

Dayuan, C., Feng, C. & Guoyu, H. (1988). Influence of "stress reversal" on rock resistivity during the loading procedure. *Acta Seismologica Sinica*, 1(3), 84–92.

Dwivedi, R. D., Singh, M., Viladkar, M. N., & Goel, R. K. (2013). Prediction of tunnel deformation in squeezing grounds. *Engineering Geology*, *161*, 55–64. https://doi.org/10.1016/j.enggeo.2013.04.005

Feng, X., & Jimenez, R. (2015). Predicting tunnel squeezing with incomplete data using Bayesian networks.

Engineering Geology, *195*, 214–224. https://doi.org/10.1016/j.enggeo.2015.06.017

Fergusson, C. L., Nutman, A. P., Mohajjel, M., & Bennett, V. C. (2016). The Sanandaj–Sirjan zone in the Neo-Tethyan suture, western Iran: Zircon U–Pb evidence of late Palaeozoic rifting of northern Gondwana and mid-Jurassic orogenesis, *Gondwana Research, 40, 43–57.* doi:10.1016/j.gr.2016.08.006

Geotomosoft. (2014). RES2DINVx64 features. 10–11. http://www.geotomosoft.com/

Ghasemi, A., & Talbot, C. J. (2006). A new tectonic scenario for the Sanandaj–Sirjan zone (Iran). *Journal of Asian Earth Sciences, 26(6), 683–693.* doi:10.1016/j.jseaes.2005.01.003

Ghazi, M. J., Moazzen, M. (2015). Geodynamic evolution of the Sanandaj-Sirjan zone, Zagros Orogen, Iran, *Turkish Journal of Earth Sciences,* 24, 513–528. https://doi.org/10.3906/yer-1404-12

Goel, R. K., Jethwa, J. L., & Paithankar, A. G. (1995). Tunneling through the young Himalayas - A case history of the Maneri-Uttarkashi power tunnel. *Engineering Geology*, *39*(1–2), 31–44. https://doi.org/10.1016/0013-7952(94)00002-J

Guan, Z., Deng, T., Du, S., Li, B., & Jiang, Y. (2012). Markovian geology prediction approach and its application in mountain tunnels. *Tunneling and Underground Space Technology*, *31*, 61–67. https://doi.org/10.1016/j.tust.2012.04.007

Gutierrez, M., & Xia, C. C. (2008). Squeezing potential of tunnels in clays and clay shales from normalized undrained shear strength, unconfined compressive strength, and seismic velocity. *Geotechnical Aspects of Underground Construction in Soft Ground – Ng, Huang & Liu.*

Hasanpour, R., Rostami, J., & Ünver, B. (2014). 3D finite difference model for simulating double shield TBM tunneling in squeezing grounds. *Tunneling and Underground Space Technology*, 40, 109–126. https://doi.org/10.1016/j.tust.2013.09.012

Hoek, E., & Marinos, P. (2000). Predicting tunnel squeezing problems in weak heterogeneous rock masses.

Part 1: Estimating rock mass strength. *Tunnels and Tunnelling International*, *Part 1-2*(2), 1–20. http://www.rockscience.com/hoek/references/H2000d.pdf.

Howland-rose, A. W. (1981). A report on a rapid reconnaissance magnetic induced polarization survey over a section of the claim group highland valley. *Centurion exploration inc*.

ISRM. (1977a). Suggested Methods for Determining the Uniaxial Compressive Strength and Deformability of Rock Materials. December, 0–3.

ISRM. (1977b). Suggested Methods for Determining water content, porosity, density, absorption, and related properties. December, 0–14.

ISRM. (1978). Suggested Methods for Determining the Strength of Rock Materials in Triaxial Compression: Revised Version 1. c.

ITASCA. (2002). FLAC2D User's Guide. *Itasca Consulting Group, Inc., Minneapolis, Minnesota 55415 USA*.

Jethwa J L, Singh B, Singh B (1984). Estimation of ultimate rock pressure for tunnel linings under squeezing rock conditions-a new approach. *In: Brown E T, Hudson J A (Eds.). Design and Performance of Underground Excavations. ISRM Symposium, Cambridge*, 231–238.

Jimenez, R., & Recio, D. (2011). A linear classifier for probabilistic prediction of squeezing conditions in Himalayan tunnels. *Engineering Geology*, *121*(3–4), 101–109. https://doi.org/10.1016/j.enggeo.2011.05.006

Khanlari, G., meybodi, R. G., & Mokhtari, E. (2012). Engineering geological study of the second part of water supply Karaj to Tehran tunnel with emphasis on squeezing problems. *Engineering Geology*, *144–145*, 9–17. https://doi.org/10.1016/j.enggeo.2012.06.001

Kovari, K., & Staus, J. (1996). Basic considerations on squeezing ground. *Rock Mechanics and Rock Engineering Journal*, *29*(4), 203–210. https://doi.org/10.1007/bf01042533

Laszlo, Z.S. (2011). The effect of fracturing on electrical resistivity and sonic wave propagation. *6th Congress of Balkan Geophysical Society Budapest Hungary*.

Li, K., Pan, B., & Horne, R. (2015). Evaluating fractures in rocks from geothermal reservoirs using resistivity at different frequencies. *39*(2000), 321–328.

Loke, M. H. (2002). Tutorial: 2-D and 3-D electrical imaging surveys. www.geoelectrical.com.

Mair, K., Elphick, S., & Main, I. (2002). Influence of confining pressure on the mechanical and structural evolution of laboratory deformation bands. *Geophysical Research Letters*, *29*(10), 49-1-49–4. https://doi.org/10.1029/2001gl013964.

Malan, D. F. (1999). Time-dependent behavior of deep-level tabular excavations in hard rock. *Rock Mechanics and Rock Engineering Journal*, 32(2), 123–155. https://doi.org/10.1007/s006030050028

Militzer, H., Rosler, R., & Losch, W. (1979). Theoretical and Experimental Investigations for Cavity Research With Geoelectrical Resistivity Methods. *Geophysical Prospecting*, *27*(3), 640–652. https://doi.org/10.1111/j.1365-2478.1979.tb00991.x

Moosavi, M., & Khazaei, S. (2003). Absolute deformation profile measurement in tunnels using relative convergence measurements. *Proceedings of 11th FIG Symposium on Deformation Measurements*, 1–6.

Palmstrom, A. (1996). Characterizing Rock Masses by the RMi for use in practical rock engineering. Part 2: some practical applications of RMi. *J. tunneling and underground space technology, 11(3),* 287–303.

Rocscience. (2004). RocSupport 1.0 tutorial manual, 1–13.

Rocscience. (2007). RocLab 1.0 tutorial manual, 1–25.

Rolia, E., & Sutjiningsih, D. (2018). Application of the geoelectric method for groundwater exploration from the surface (A literature study). *AIP Conference Proceedings, 1977, 020018.* https://doi.org/10.1063/1.5042874

Sandler, J., Li, Y., Horne, R. N., & Li, K. (2009). Effects of Fracture and Frequency on Resistivity in Different Rocks. E*UROPEC/EAGE Conference and Exhibition, Amsterdam, the Netherlands, June*, 8–11, *SPE 119872*. https://doi.org/10.2118/119872-MS

Sasaki, Y. (1992). Resolution of Resistivity Tomography Inferred From Numerical Simulation. *Geophysical Prospecting*, 40(4), 453–463. https://doi.org/10.1111/j.1365-2478.1992.tb00536.x

Scintrex limited. (1995). CG–3/3M autograph automated gravity meter-operator manual. Version 5.

Shen, J., Karakus, M., & Xu, C. (2012). A comparative study for empirical equations in estimating deformation modulus of rock masses. *Tunneling and Underground Space Technology*, *32*, 245–250. https://doi.org/10.1016/j.tust.2012.07.004

Shrestha, G. L., & Broch, E. (2008). Influences of the valley morphology and rock mass strength on tunnel convergence: With a case study of Khimti 1 headrace tunnel in Nepal. *Tunneling and Underground Space Technology*, 23(6), 638–650. https://doi.org/10.1016/j.tust.2007.12.006

Singh, B., Jethwa, J. L., Dube, A. K., & Singh, B. (1992). Correlation between observed support pressure and rock mass quality. *Tunneling and Underground Space Technology Incorporating Trenchless*, 7(1), 59–74. https://doi.org/10.1016/0886-7798(92)90114-W

Singh, B., Viladkar, M. N., Samadhiya, N. K., & Mehrotra, V. K. (1997). Rock mass strength parameters mobilized in tunnels. *Tunneling and underground space technology*, 12(1), 47-54.

Sun, Y., Feng, X., & Yang, L. (2018). Predicting Tunnel Squeezing Using Multiclass Support Vector Machines. *Hindawi, Advances in Civil Engineering*, 17–20. https://doi.org/10.1155/2018/4543984

Swannell, N., Palmer, M., Barla, G., & Barla, M. (2016). The geotechnical risk management approach for TBM tunneling in squeezing ground conditions. *Tunneling and Underground Space Technology*, *57*, 201–210. https://doi.org/10.1016/j.tust.2016.01.013

Thut, A., Naterop, D., Steiner, P., & Stolz, M. (2000). Tunneling in squeezing rock-yielding elements and face control, *Solexperts AG Mettlenbachstrasse 25 CH – 8617 Mönchaltorf Switzerland*.

Vrakas, A., Dong, W., Anagnostou, G. (2017). Elastic deformation modulus for estimating convergence when tunneling through squeezing ground. *Geotechnique, 68(8),* 713-728. https://doi.org/10.1680/jgeot.17.p.008

Whiteley, R. J. (2006). Applications of engineering geophysics to underground space. *IAEG 603*, 1–7.

Wood, A. M. M. (1972). Tunnels for roads and motorways. *Quarterly Journal of Engineering Geology*, *5*(1–2), 111–126. https://doi.org/10.1144/GSL.QJEG.1972.005.01.12

Zayandab Engineering Consulting Company. (2006). Geotechnical report of Isfahan water transition (Golab) tunnel (In Persian).

Zayandab Engineering Consulting Company. (2010). Geotechnical report of Beheshtabad tunnel (In Persian).